

# Acid Sulfate Soils Research Program

Lower Lakes Hydro-Geochemical Model Development  
and Assessment of Acidification Risks

Report 6 | Part 2 of 4 | October 2010



## 6.2 Lake Alexandrina (River Murray-Clayton): validation (Jan 2008 – Sep 2009)

### Lake physical properties

The water levels are accurately predicted and capture the seasonal trends in lake elevation (Figure 6.13). The surface temperatures with the above configuration were well predicted throughout the simulation period (Figure 6.14) and compared well with both the EPA water quality data and the real-time DFW loggers. No spatial variability was seen in the observed temperature data or in the model. For salinity however, (plotted as electrical conductivity at 25°C, Figure 6.15), there is a notable horizontal gradient across the lake and the model generally captured the trends in the field data well. An exception was the prediction at Clayton, which could be due to the Finnis boundary condition, as is discussed separately in Section 6.3. Previous applications of ELCOM to the lower lakes have also reported accurate prediction of salinity gradients across the system (Hipsey et al., 2009).

### Nutrients and Chl-a

Dissolved Oxygen showed little difference across the domain and the lake remains oxygenated and the concentration varies in line with solubility differences (Figure 6.16). The DOC level follows a noticeable seasonal trend (Figure 6.17) that is captured by the model, although the concentration is over predicted at northern lake stations in the summer. Since the conservative ions like Cl are predicted well, this would imply evapo-concentration levels are well-captured (see below), and there is an under prediction on DOC decay during the summer period, as was the case also in Lake Albert. NH<sub>4</sub> and NO<sub>3</sub> levels are low throughout the period (Figure 6.18-6.19). TN however is quite high and is reasonably captured by the model except for some over concentration in the summer (Figure 6.20), likely for similar reasons as DOC – that is DON mineralization (and subsequent denitrification) is being under predicted. PO<sub>4</sub> is well predicted and TP is similar in trend as TN. Total Chlorophyll-a (Figure 6.23) is predicted to be high by the model with only limited data available from the profiles conducted by SA Water. These are notorious for poor prediction of Chlorophyll-a magnitude, particularly when not calibrated, so it is not unreasonable that the levels reported here by the model are higher than those reported by the profiler. There is a strong seasonal trend of Chl-a increase that follows the trend in temperature, with higher concentrations at the end of summer and low concentrations in winter.

### Lake Geochemistry

As in the Lake Albert simulations, the role of solubility control of alkalinity by calcite/aragonite was also important in Lake Alexandrina, however, a slight adjustment of the calcite solubility product was required relative to the Albert simulations for the model to more accurately reflect the field data for DIC (Figure 6.24,  $K_{sp} = -8.2$ ). Ca was well predicted across the lake although was under-predicted at Clayton. This was found to be due to overly high flow rate coming in Finnis erroneously (note this error was updated in the Currency/Finnis high resolution domain simulation described below). This under-prediction at Clayton is reflected in all the other major ions.

The remaining geochemical variables (Cl & Na, Figure 6.25-6.26; Mg & SO<sub>4</sub>, Figure 6.27-6.28; pH and CHGBAL, Figure 6.29-6.30) were all predicted well by the model. The dissolved metals were also simulated but were near zero during the validation period, as expected (Figure 6.31-6.33).

The large scale model domain (AA) presented in this sub-section poorly resolves the Currency/Finnis tributaries and disconnected pools during the summer of 2009. It is therefore not considered suitable for high resolution prediction of the pools that became acidic during 2009. Nonetheless we report here the pH predictions generated by this coarse resolution domain in this sub-region to see its performance at this scale (Figure 6.33). The model does predict acidification during May of 2009 in the currency tributary, but the pools dry out too early. This is not surprising given the coarse nature of the grid at this location, but the general trend of acidification at the appropriate time gives us some confidence that model is able to resolve dynamics even at this larger scale.

The spatial distribution of soil acidity predicted by the model (Figure 6.35) compares favourably with Fitzpatrick et al. (2010) TAA and surface soil pH maps that highlight areas of high acidity in the north-western reaches, on the south-western margins, Loveday Bay, and patches elsewhere around the lake edge.

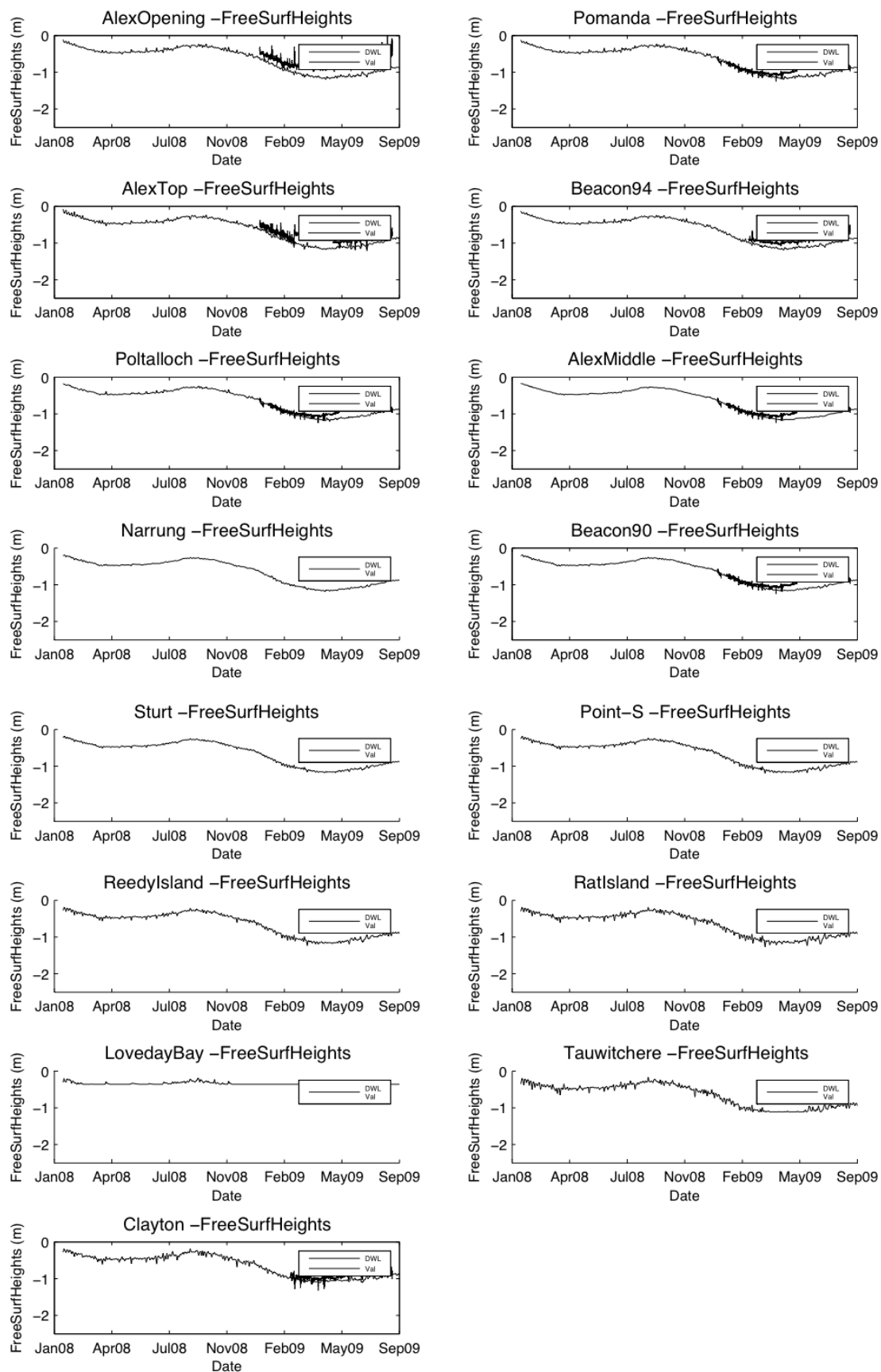


Figure 6.13: Comparison of modelled (Val) and measured (DFW) surface water elevation (mAH) for 15 stations in Lake Alexandrina from the River Murray entrance to Clayton.

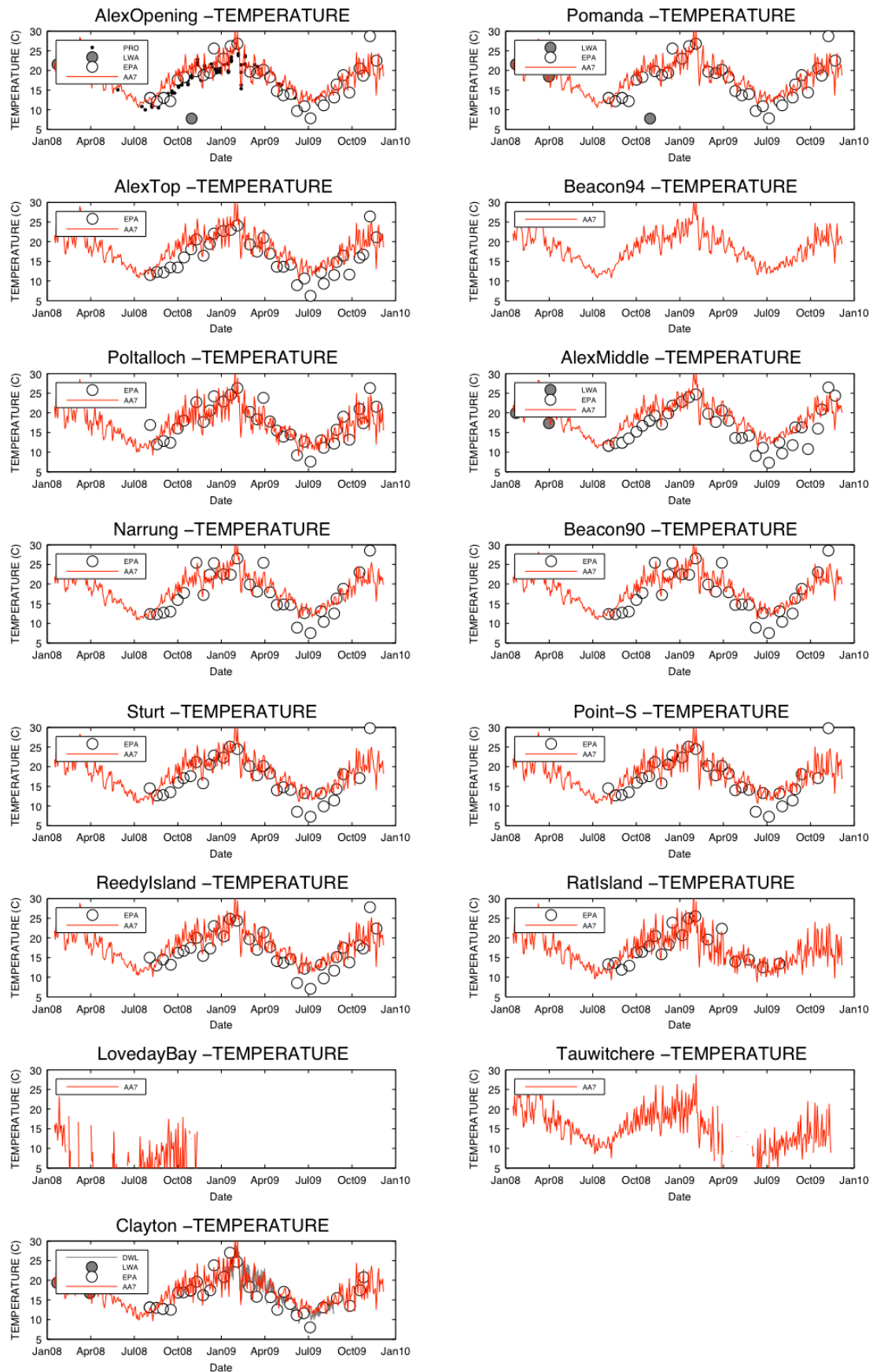


Figure 6.14: Comparison of modelled (Val) and measured (DFW and EPA) temperature data (°C) for 15 stations in Lake Alexandrina from the River Murray entrance to Clayton.

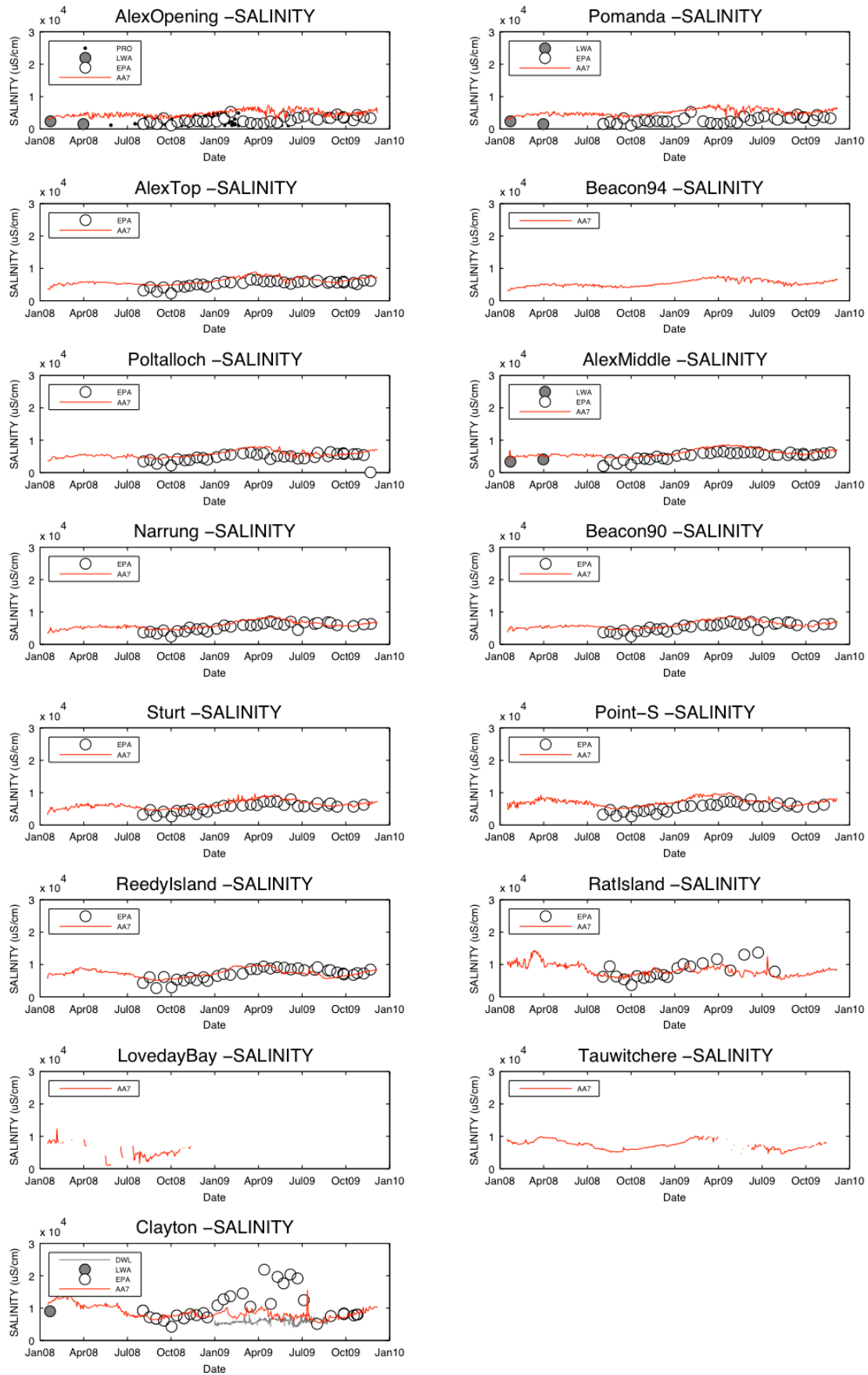


Figure 6.15: Comparison of modelled (Val) and measured (DFW and EPA) salinity/EC data (uS cm<sup>-1</sup>) for 15 stations in Lake Alexandrina from the River Murray entrance to Clayton.

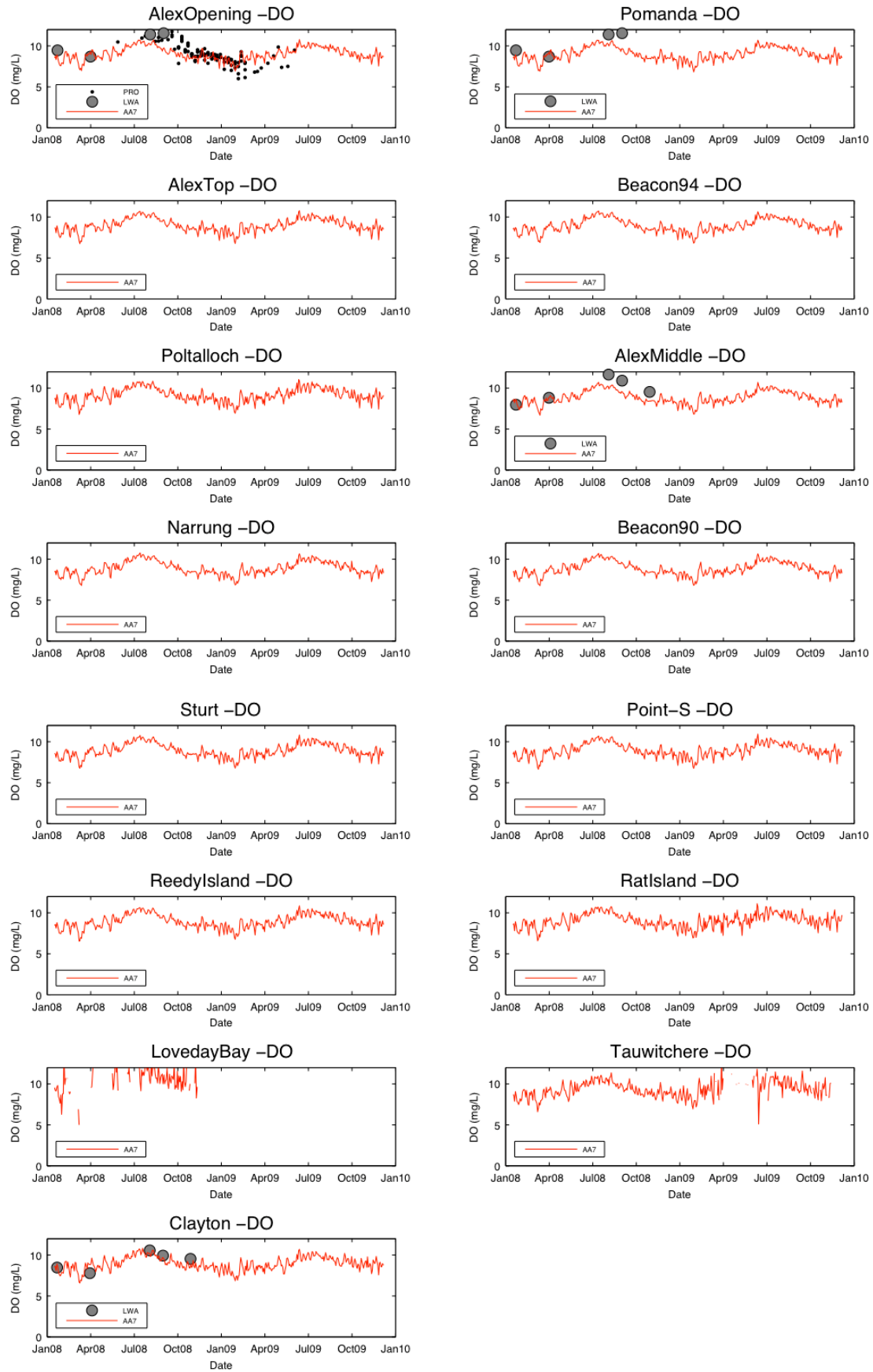


Figure 6.16: Comparison of modelled (Val) and measured (SAWater profile data, PRO) dissolved oxygen data ( $\text{mg L}^{-1}$ ) for 15 stations in Lake Alexandrina from the River Murray entrance to Clayton.

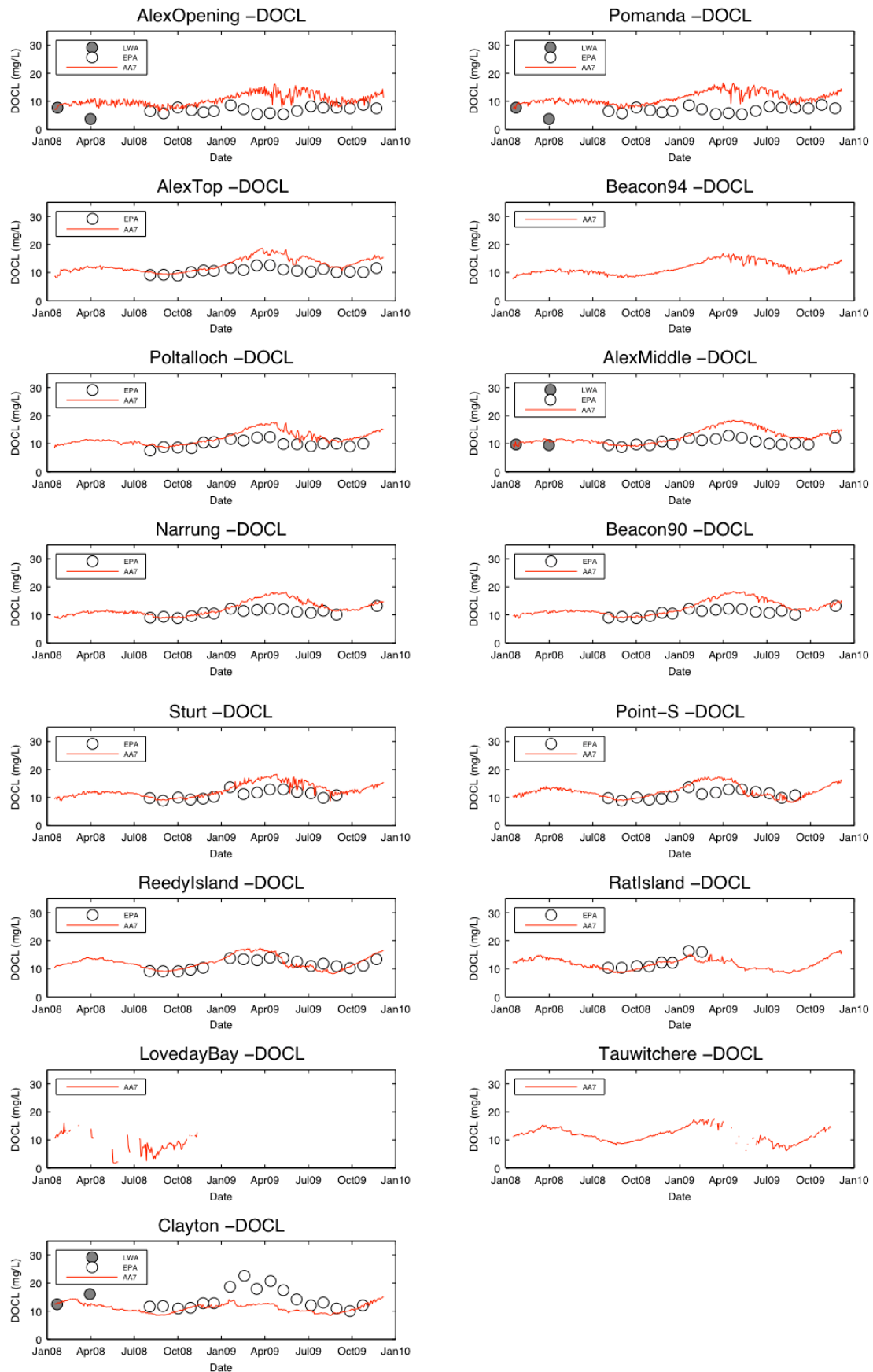


Figure 6.17: Comparison of modelled (Val) and measured (EPA) dissolved organic carbon (DOCL) data (mg C L<sup>-1</sup>) for 15 stations in Lake Alexandrina from the River Murray entrance to Clayton.

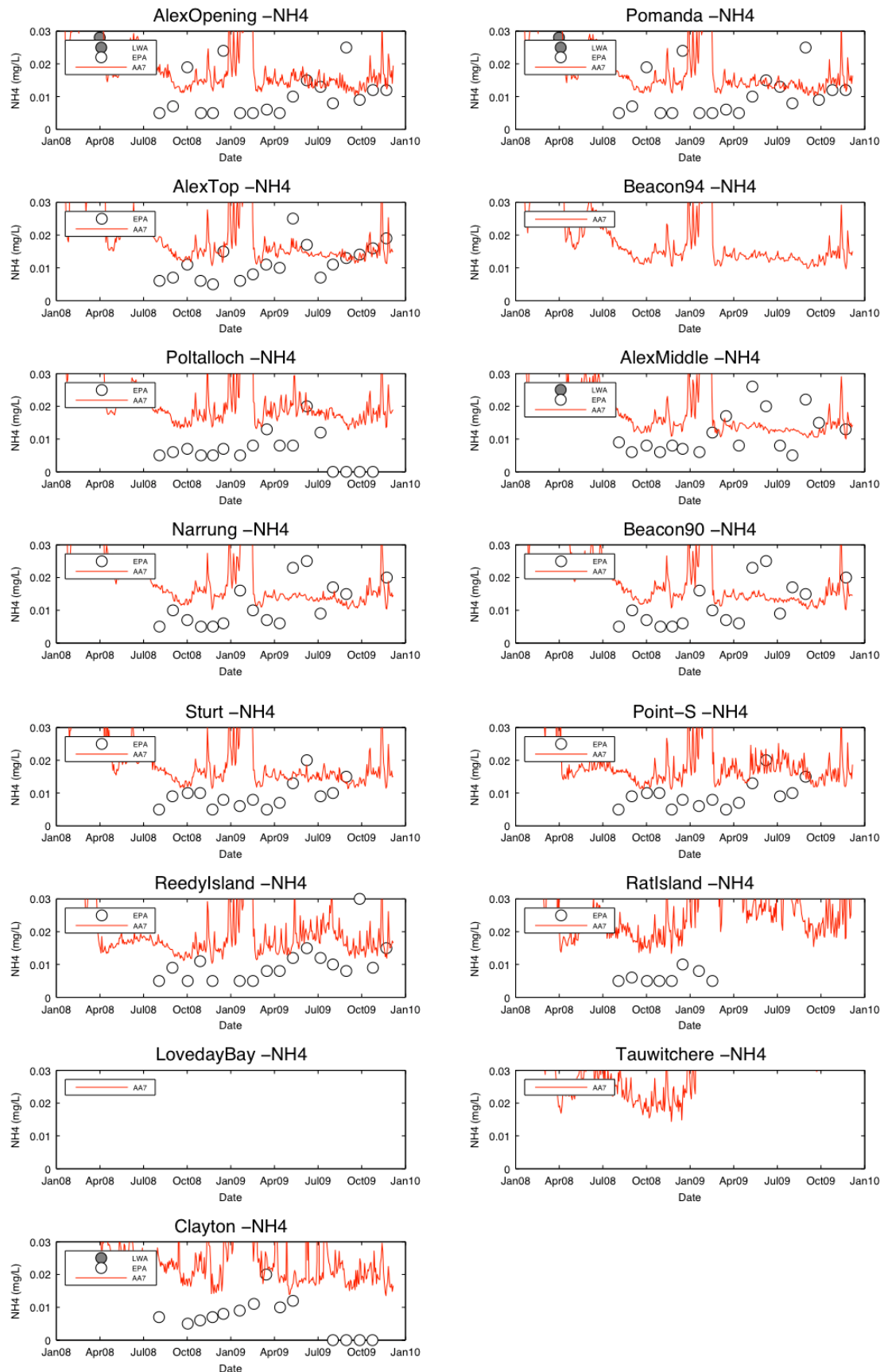


Figure 6.18: Comparison of modelled (Val) and measured (EPA) ammonium (NH4) data (mg N L<sup>-1</sup>) for 15 stations in Lake Alexandrina from the River Murray entrance to Clayton.

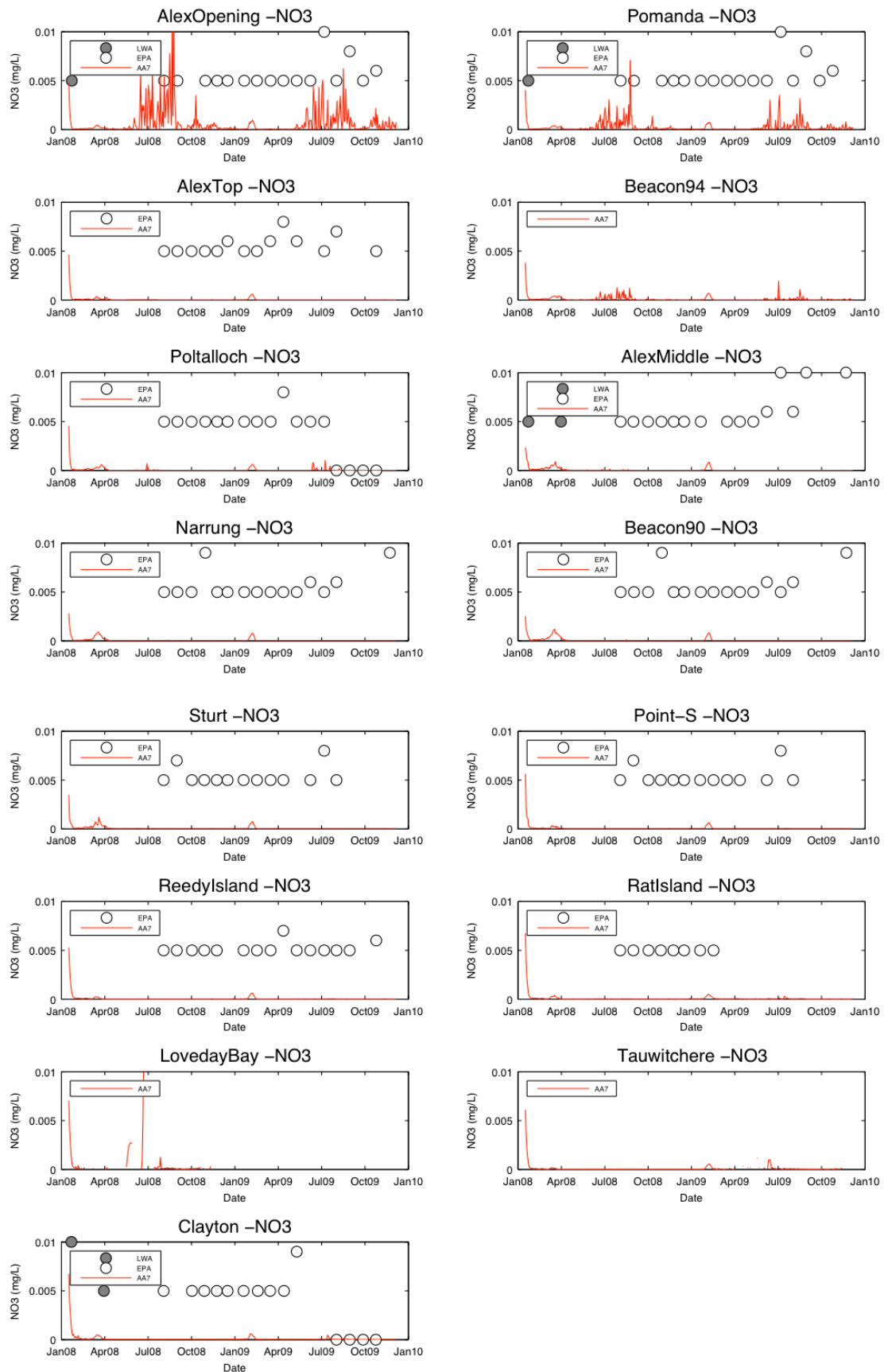


Figure 6.19: Comparison of modelled (Val) and measured (EPA) nitrate+nitrite (NO<sub>3</sub>) data (mg N L<sup>-1</sup>) for 15 stations in Lake Alexandrina from the River Murray entrance to Clayton. Note that the NO<sub>3</sub> results were often below detection limit.

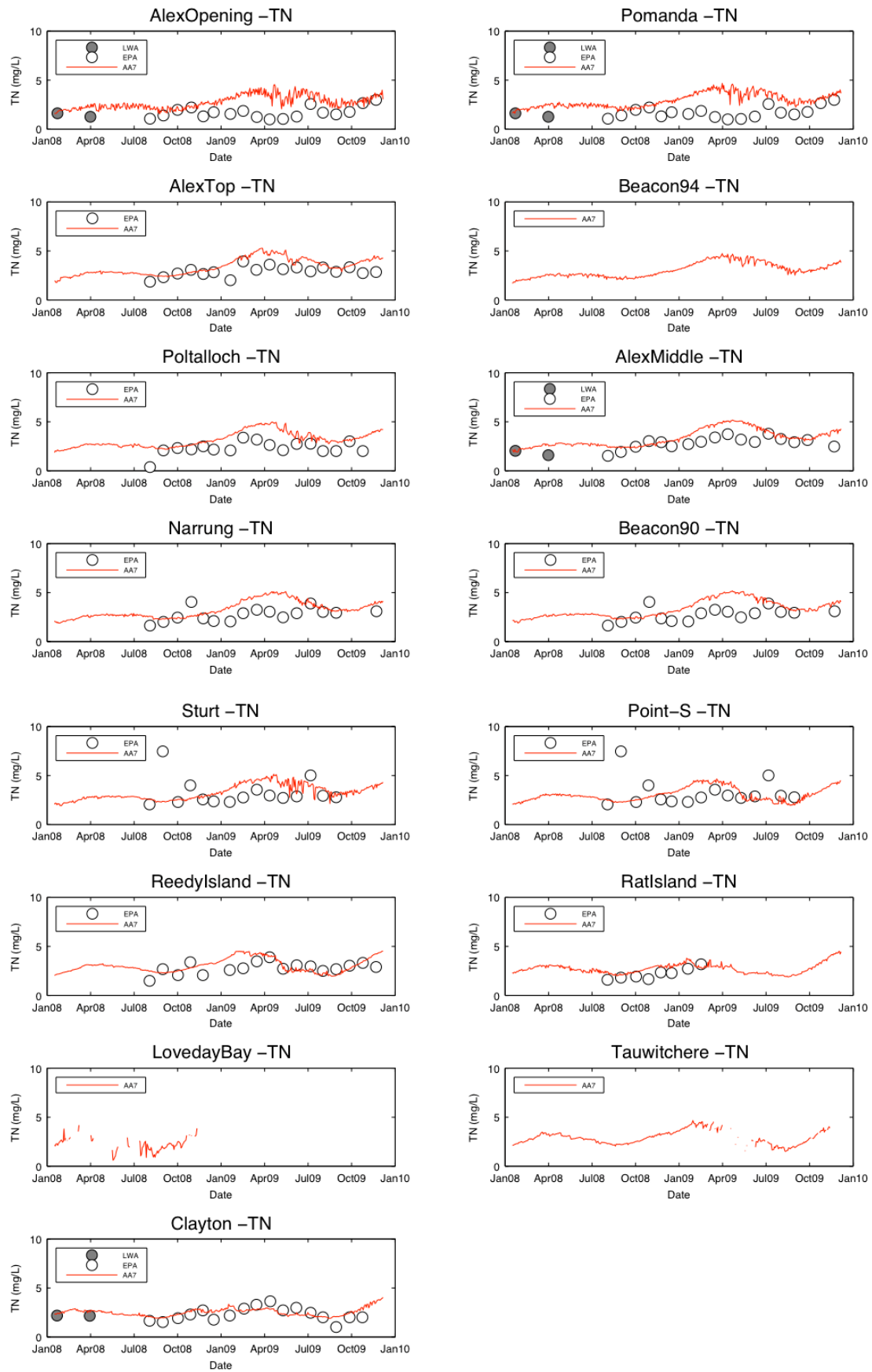


Figure 6.20: Comparison of modelled (Val) and measured (EPA) total nitrogen (TN) data (mg N L<sup>-1</sup>) for 15 stations in Lake Alexandrina from the River Murray entrance to Clayton.

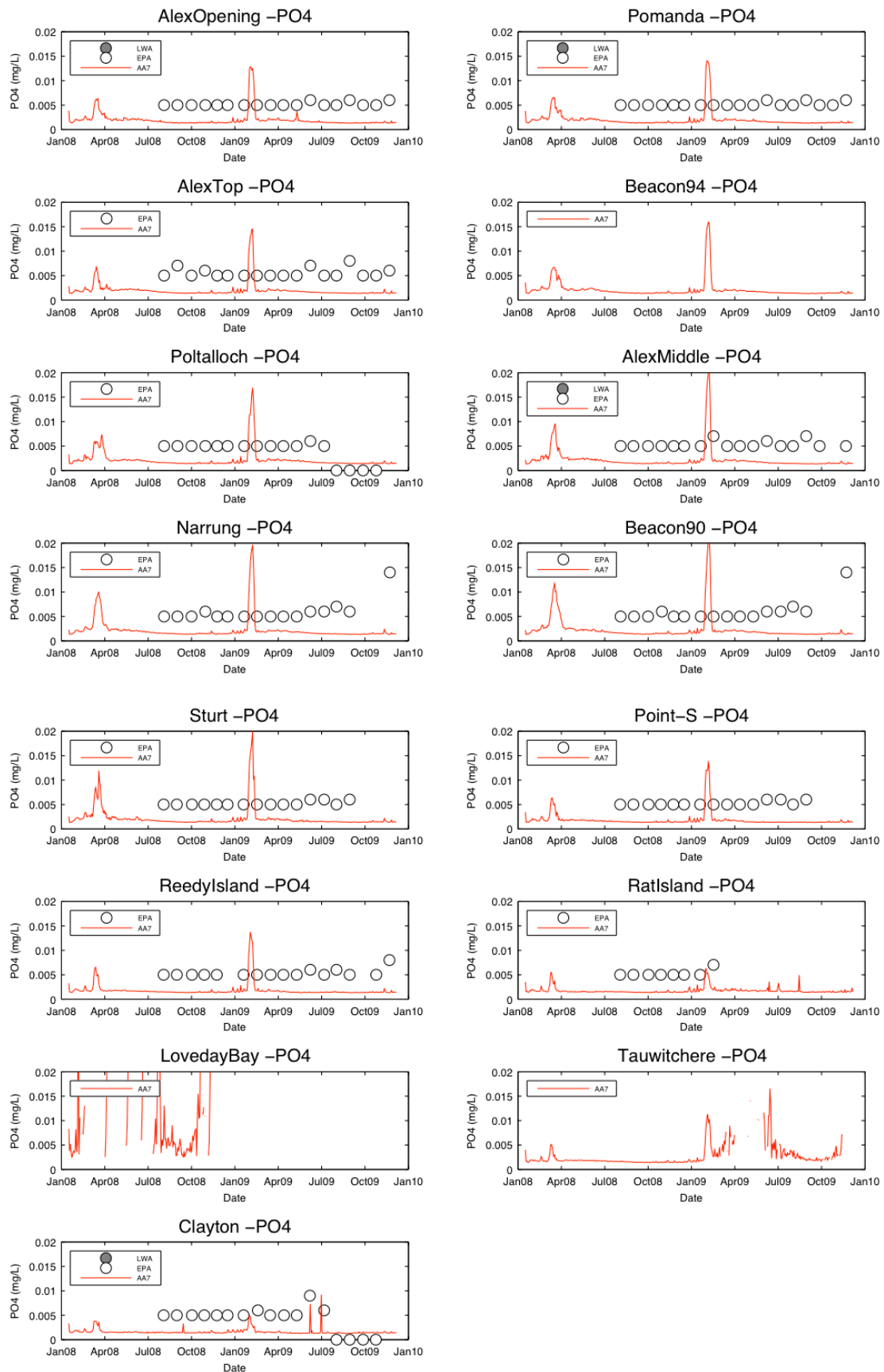


Figure 6.21: Comparison of modelled (Val) and measured (EPA) ortho-phosphate (PO<sub>4</sub>) data (mg P L<sup>-1</sup>) for 15 stations in Lake Alexandrina from the River Murray entrance to Clayton. Note that the PO<sub>4</sub> results were often below detection limit.

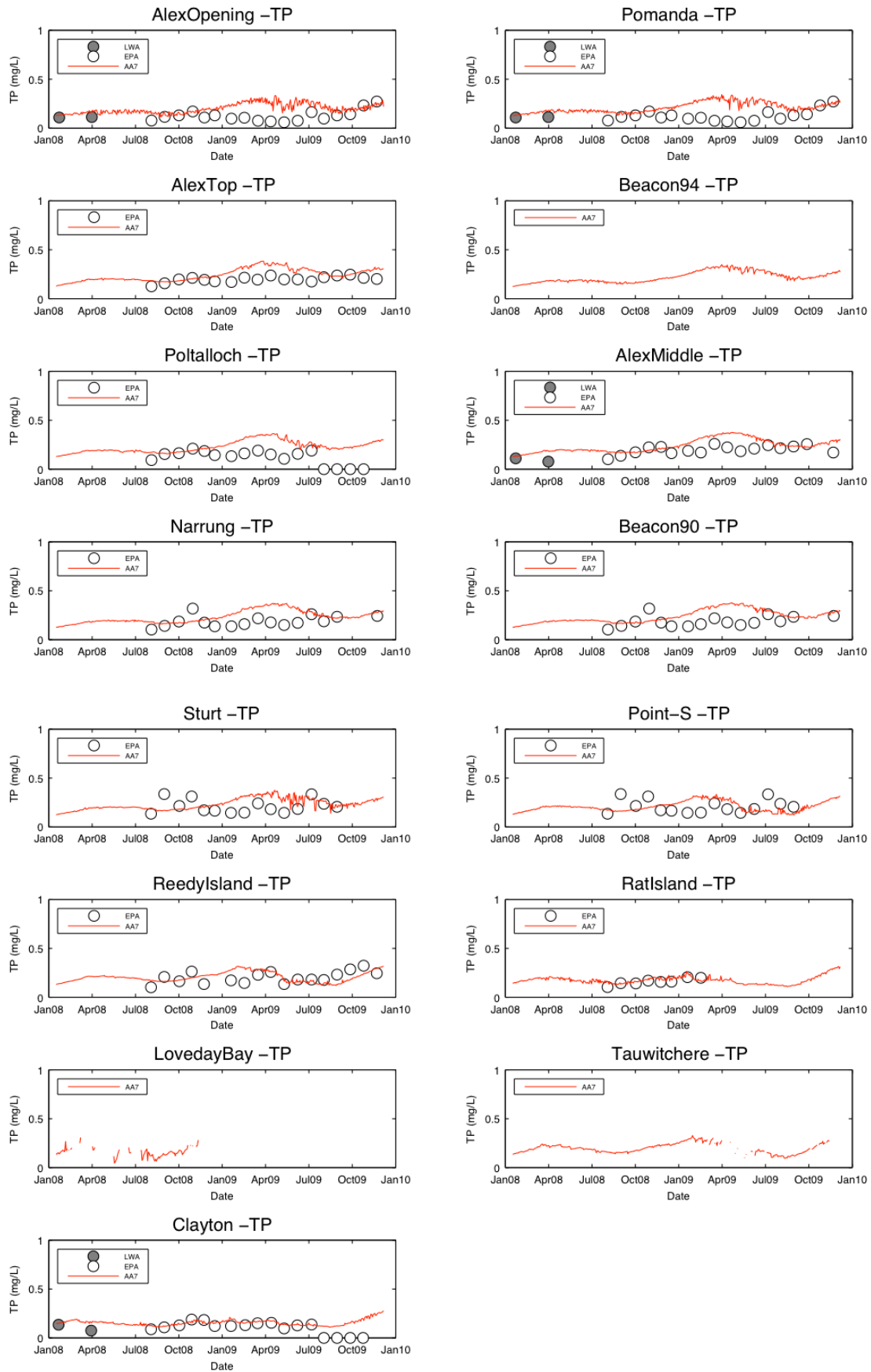


Figure 6.22: Comparison of modelled (Val) and measured (EPA) total phosphorus (TP) data ( $\text{mg P L}^{-1}$ ) for 15 stations in Lake Alexandrina from the River Murray entrance to Clayton.

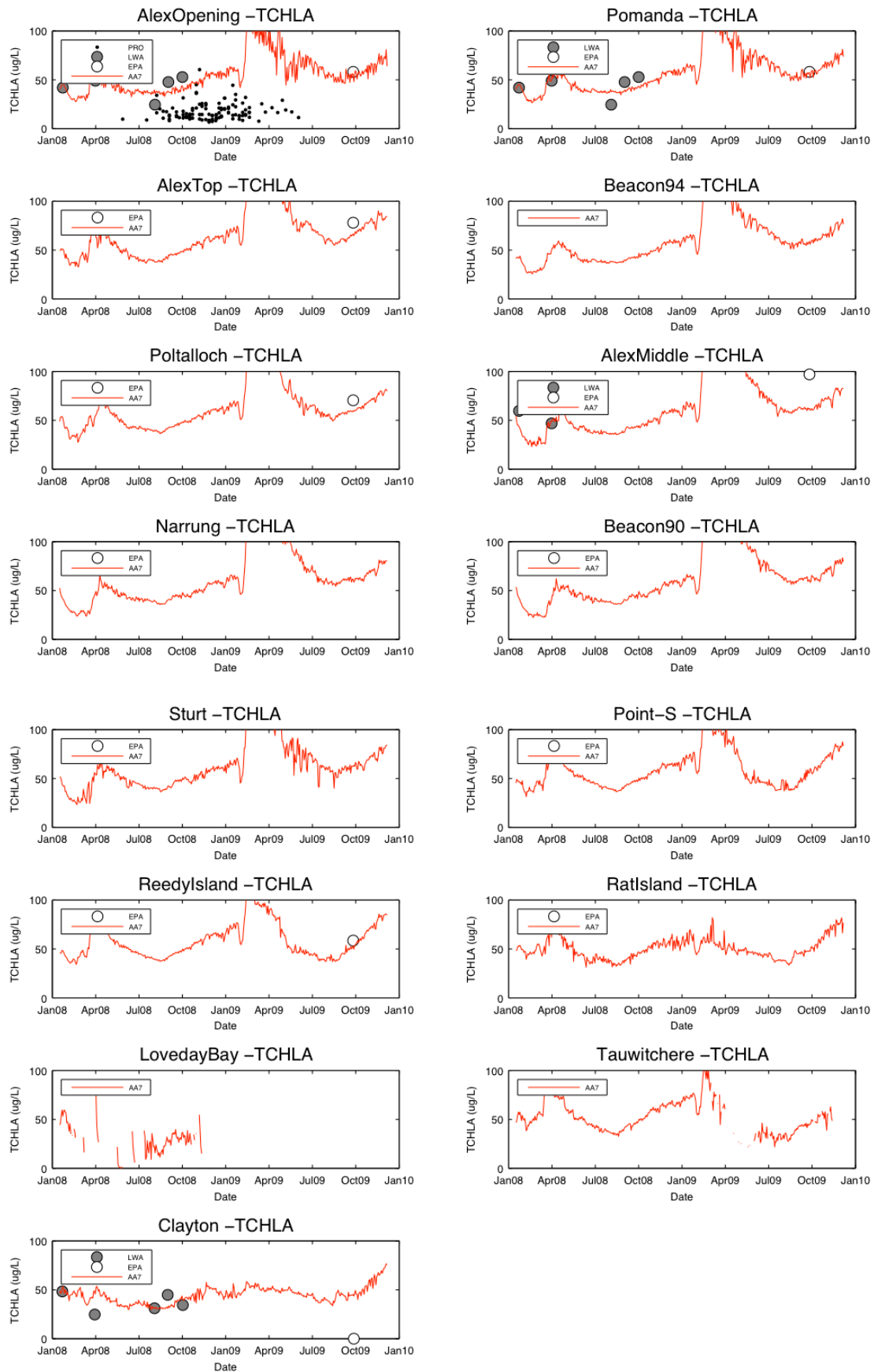


Figure 6.23: Comparison of modelled (Val) and measured (EPA) chlorophyll-a (TCHLA) data ( $\mu\text{g chl-a L}^{-1}$ ) for 15 stations in Lake Alexandrina from the River Murray entrance to Clayton.

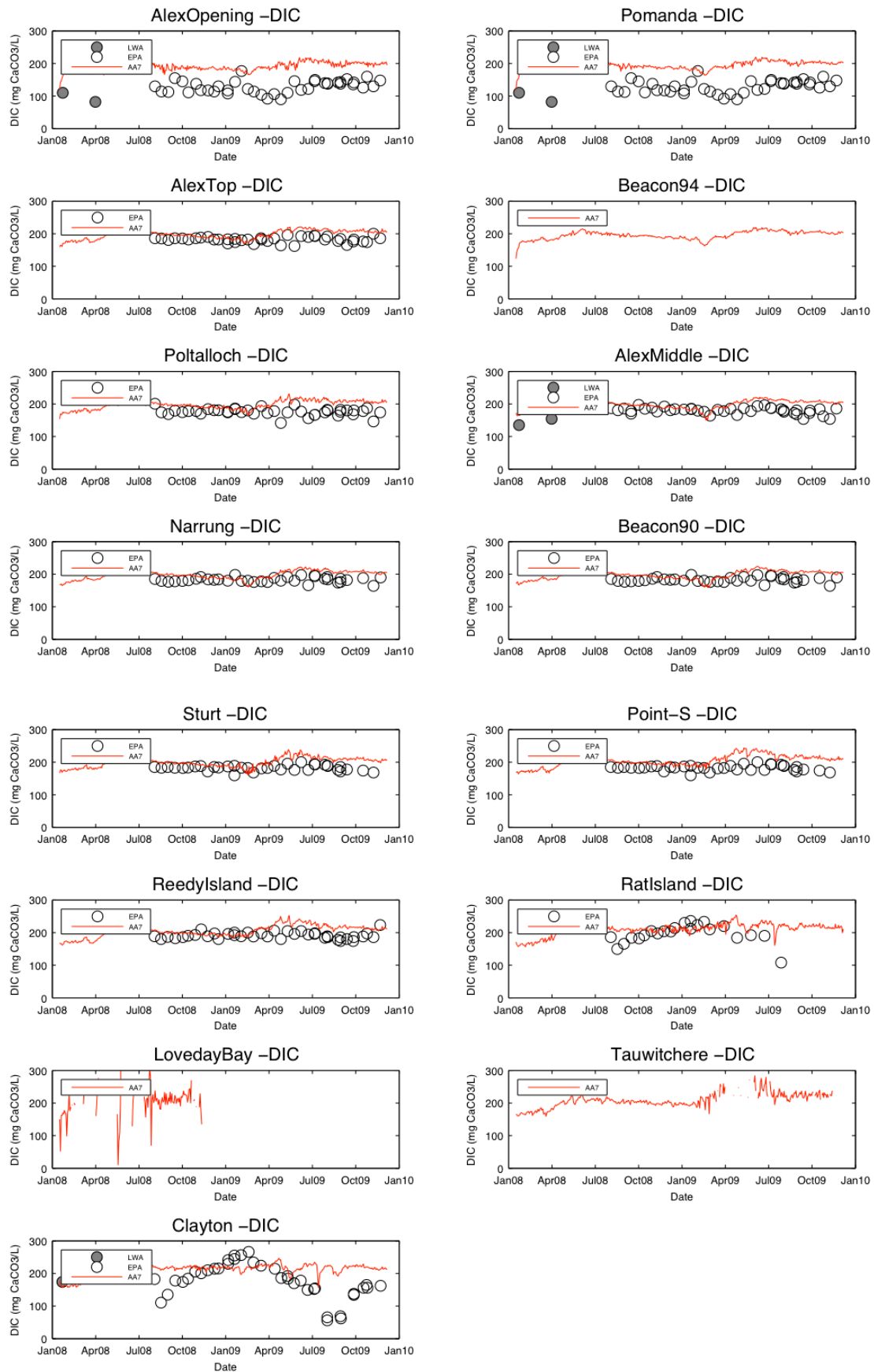


Figure 6.24: Comparison of modelled (Val) and measured (EPA) dissolved carbonate alkalinity (DIC) data (mg CaCO<sub>3</sub> L<sup>-1</sup>) for 15 stations in Lake Alexandrina from the River Murray entrance to Clayton.

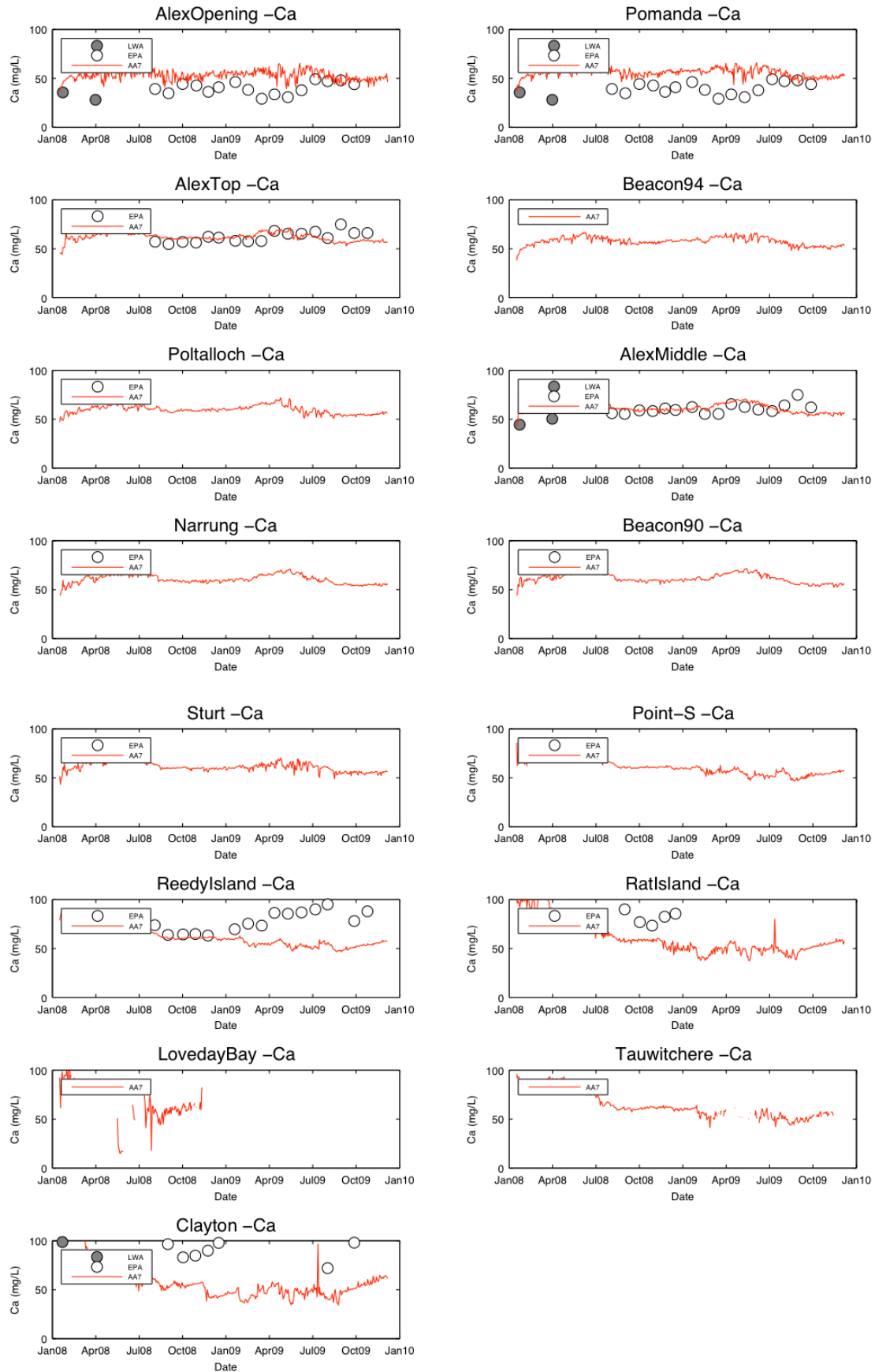


Figure 6.25: Comparison of modelled (Val) and measured (EPA) calcium (Ca) data ( $\text{mg L}^{-1}$ ) for 15 stations in Lake Alexandrina from the River Murray entrance to Clayton.

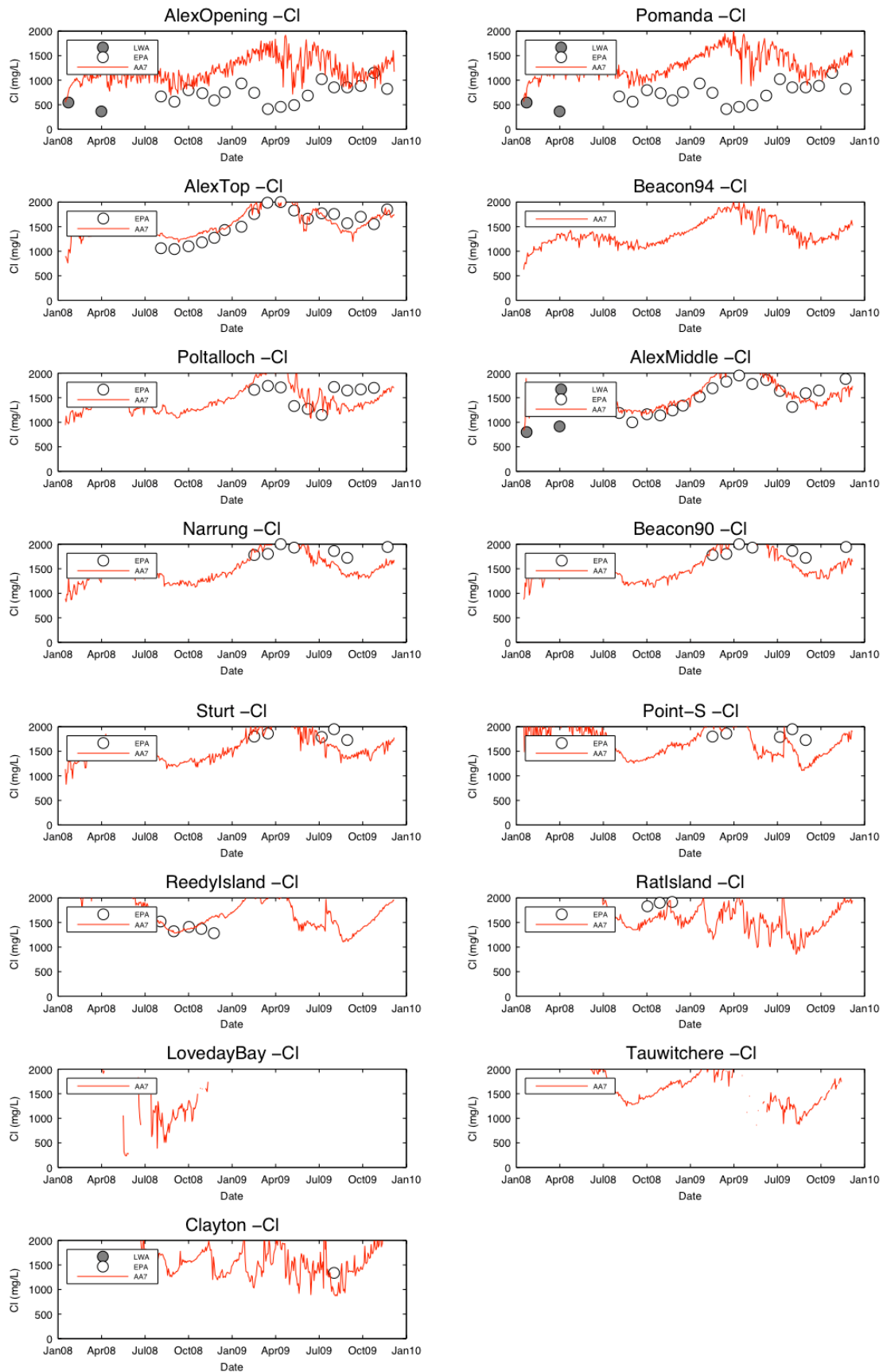


Figure 6.26: Comparison of modelled (Val) and measured (EPA) chloride (Cl) data ( $\text{mg L}^{-1}$ ) for 15 stations in Lake Alexandrina from the River Murray entrance to Clayton.

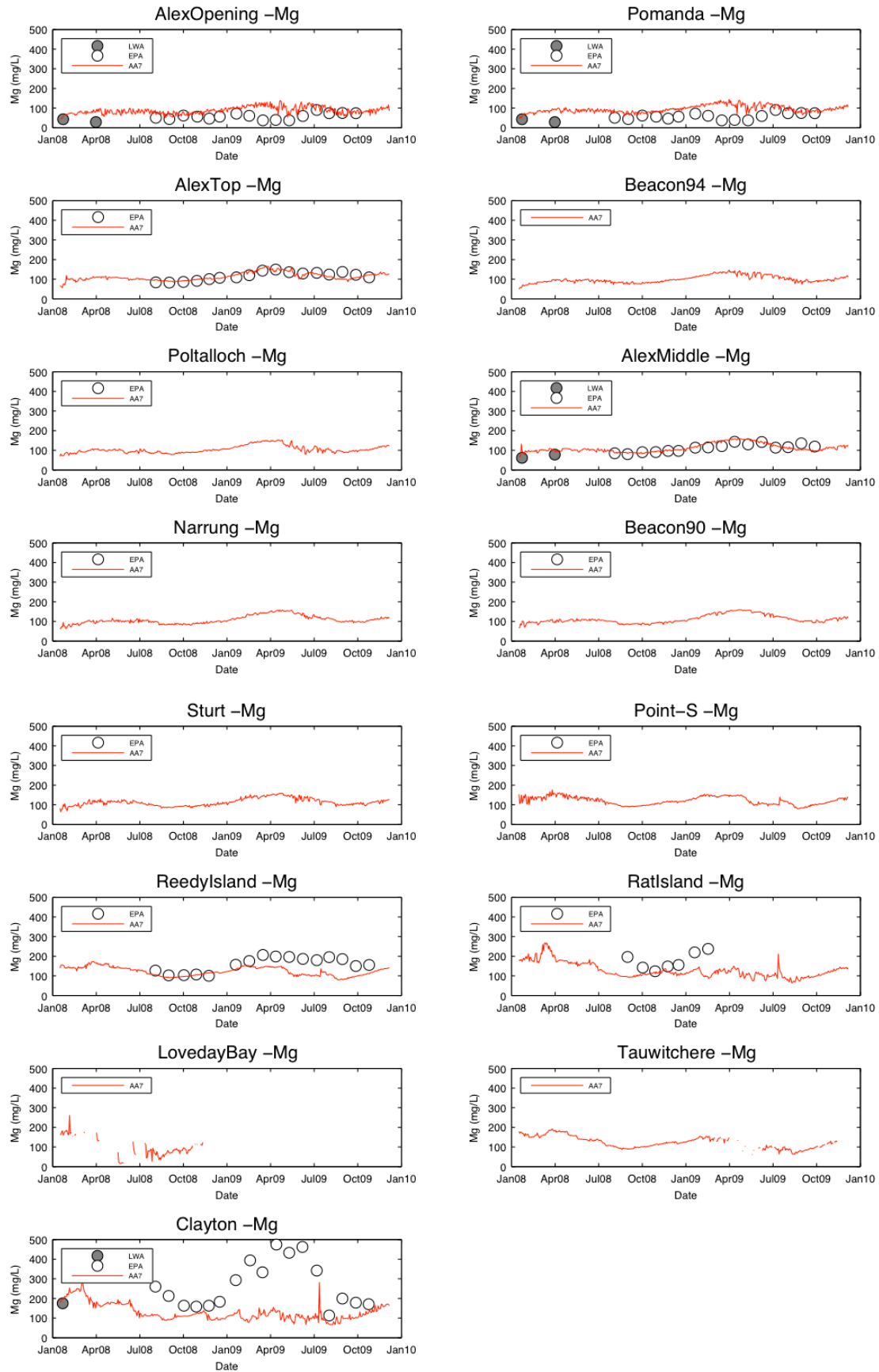


Figure 6.27: Comparison of modelled (Val) and measured (EPA) magnesium (Mg) data ( $\text{mg L}^{-1}$ ) for 15 stations in Lake Alexandrina from the River Murray entrance to Clayton.

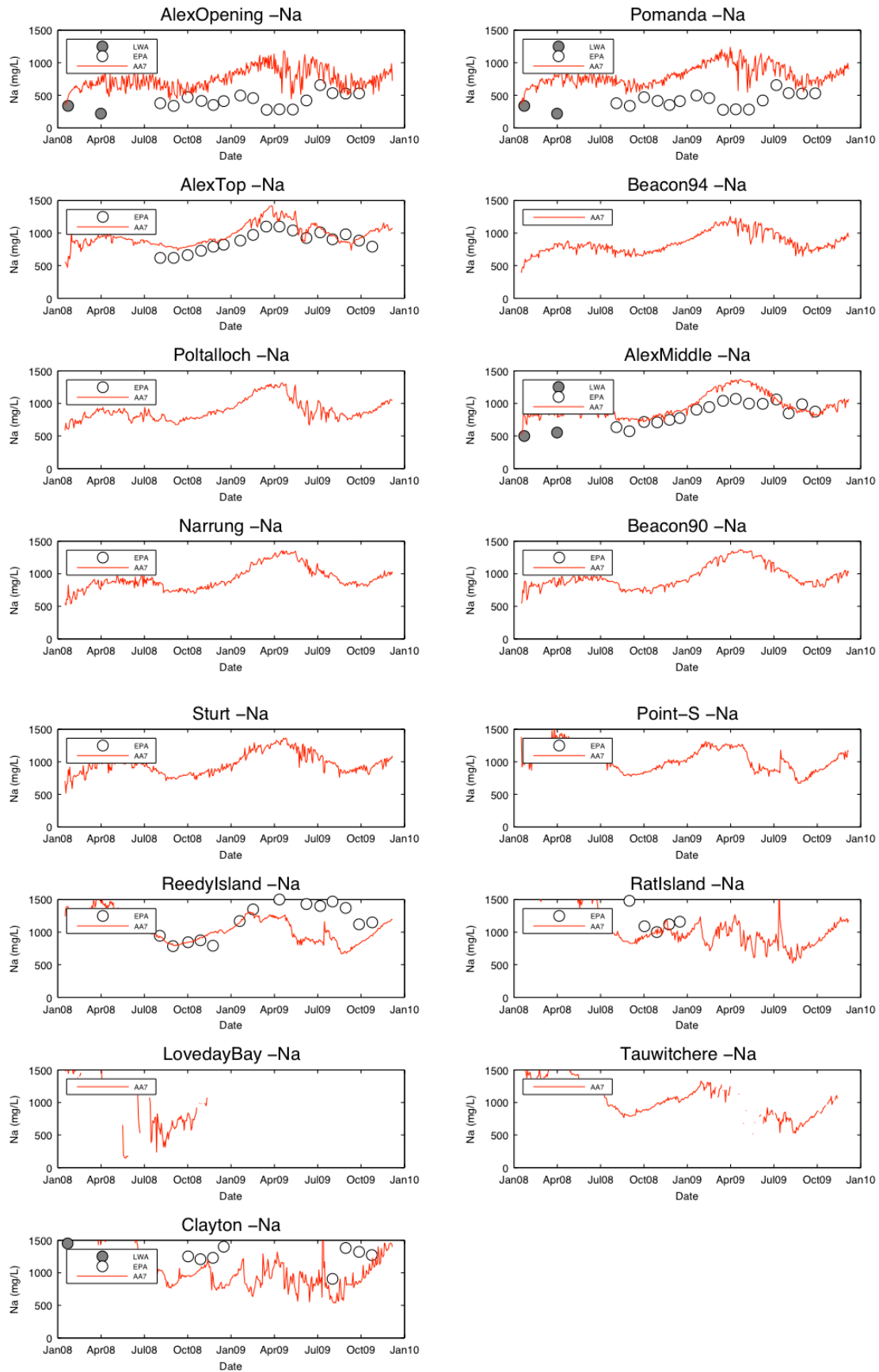


Figure 6.28: Comparison of modelled (Va) and measured (EPA) sodium (Na) data ( $\text{mg L}^{-1}$ ) for 15 stations in Lake Alexandrina from the River Murray entrance to Clayton.

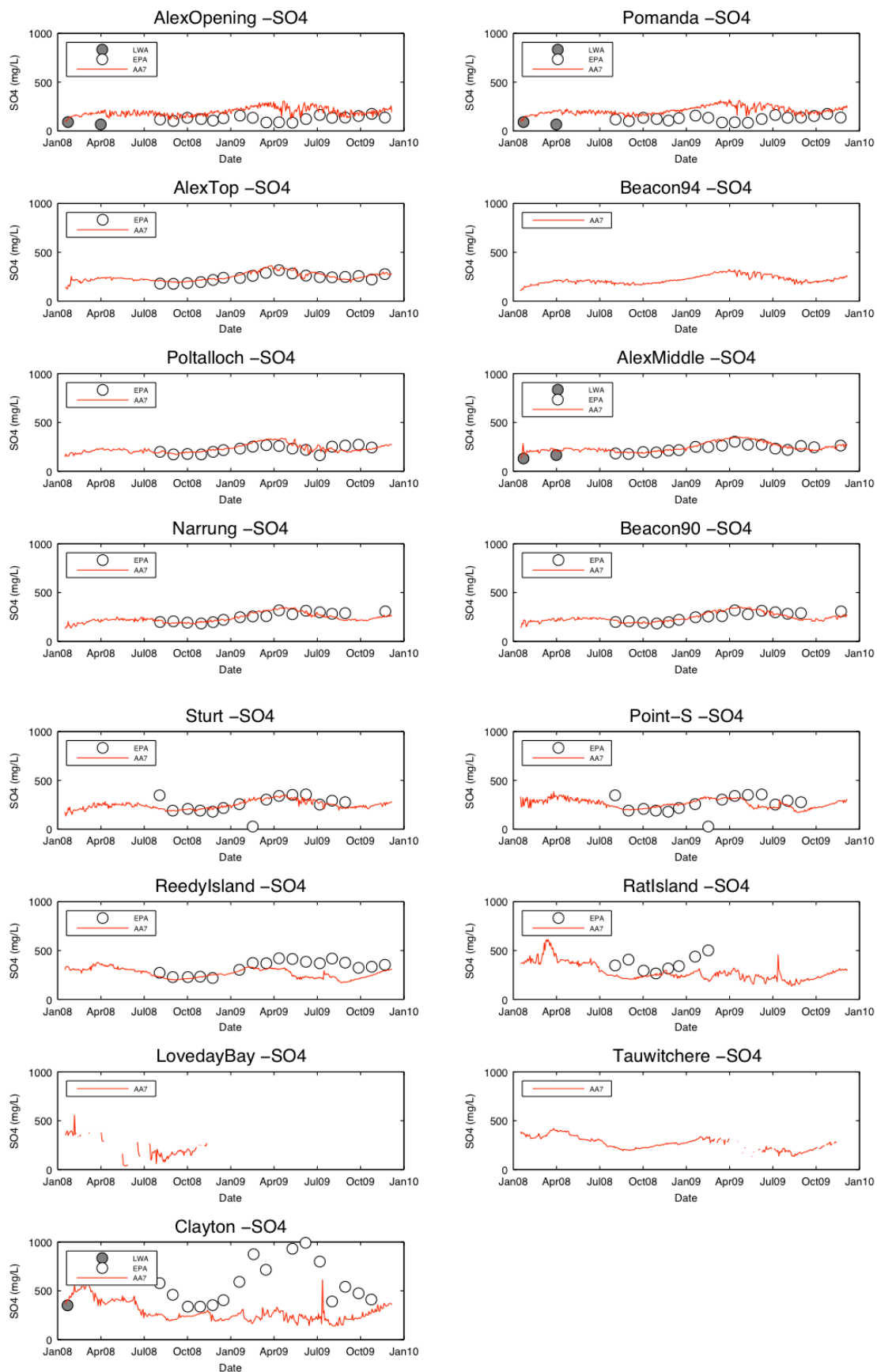


Figure 6.29: Comparison of modelled (Val) and measured (EPA) sulphate (SO<sub>4</sub>) data (mg SO<sub>4</sub> L<sup>-1</sup>) for 15 stations in Lake Alexandrina from the River Murray entrance to Clayton.

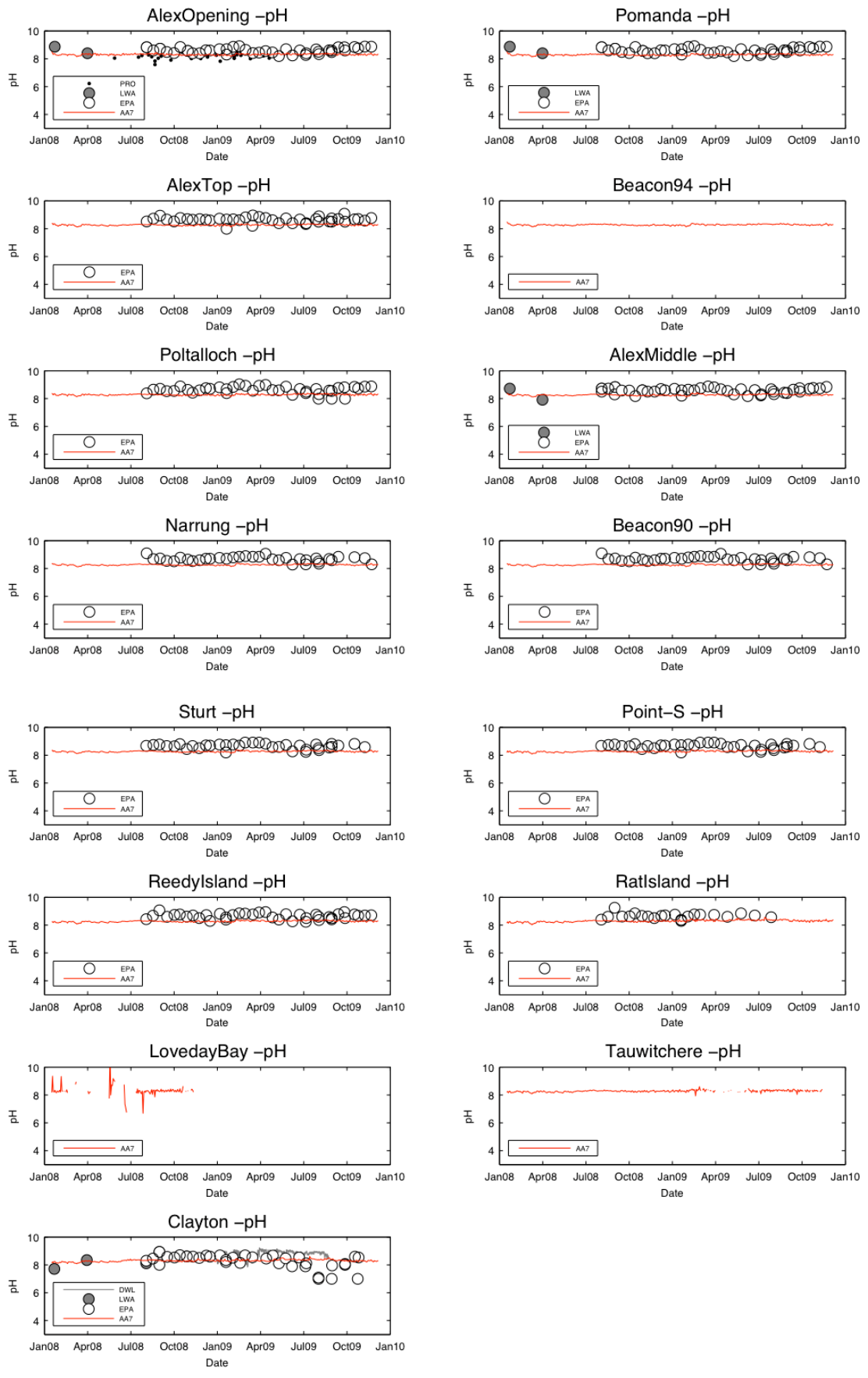


Figure 6.30: Comparison of modelled (Val) and measured (EPA) pH data for 15 stations in Lake Alexandrina from the River Murray entrance to Clayton.

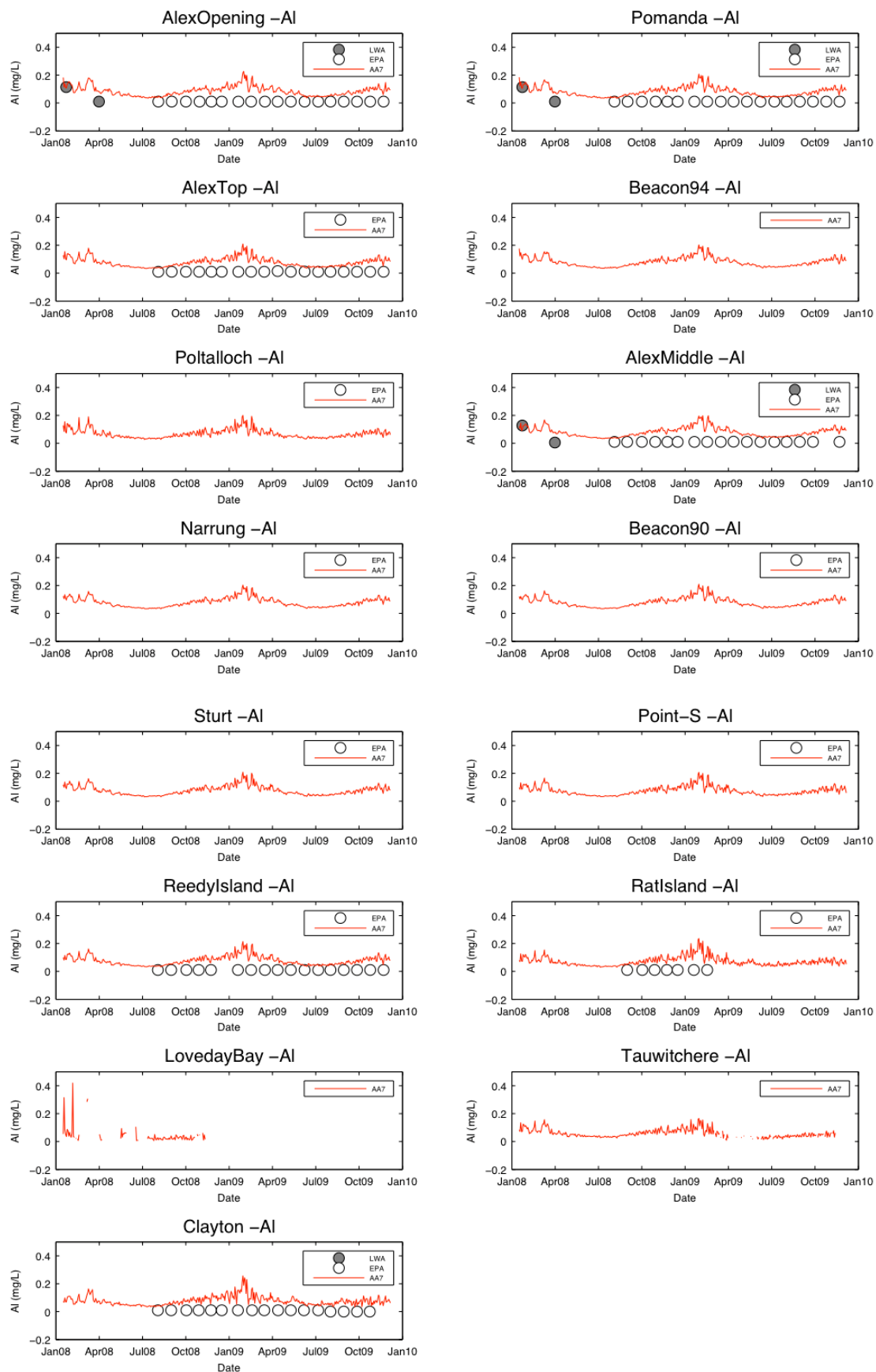


Figure 6.31: Comparison of modelled ( $V_{Al}$ ) and measured (EPA) dissolved aluminium (Al) data ( $\text{mg L}^{-1}$ ) for 15 stations in Lake Alexandrina from the River Murray entrance to Clayton.

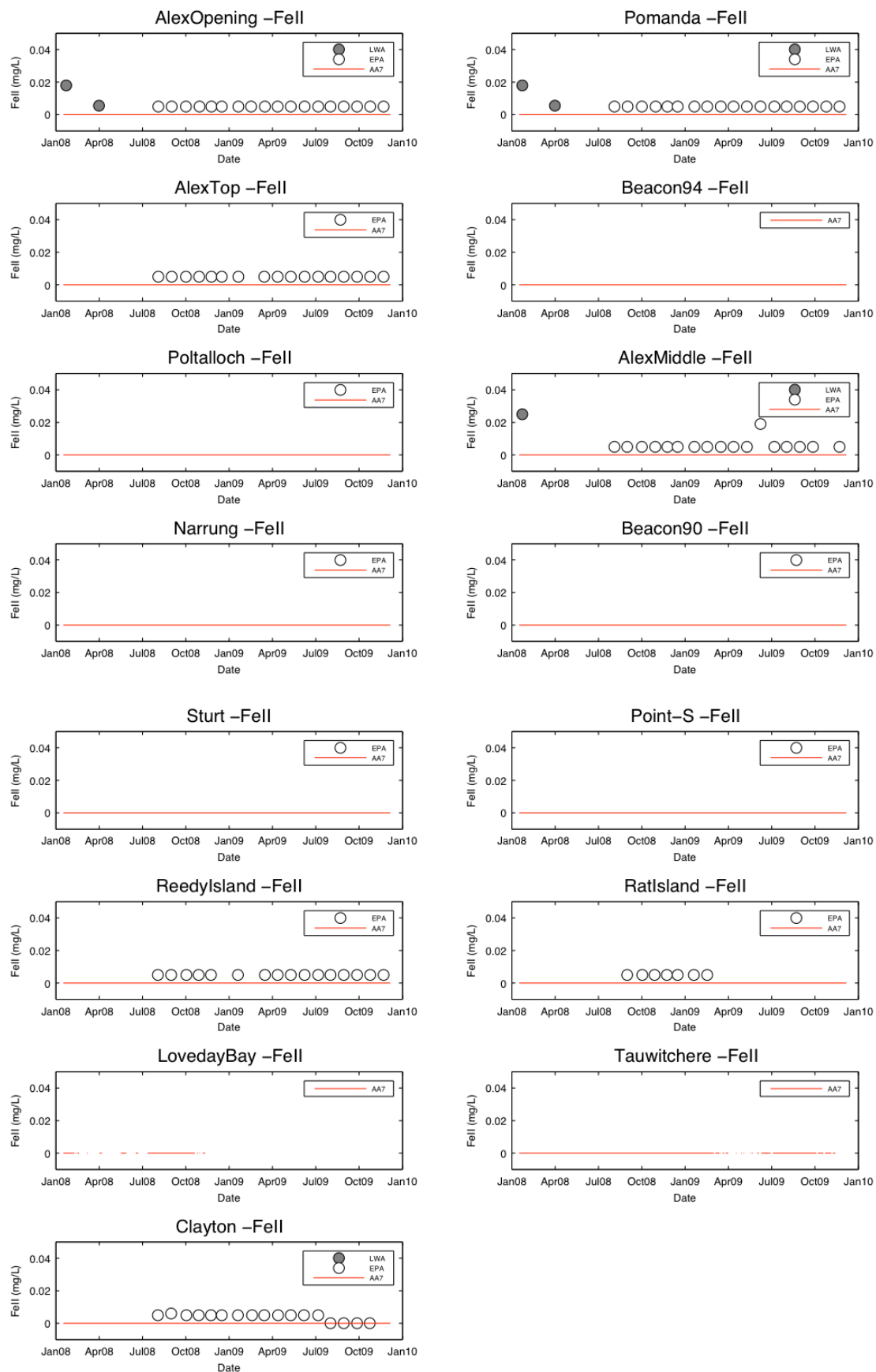


Figure 6.32: Comparison of modelled (Val) and measured (EPA) dissolved ferrous iron (Fell) data ( $\text{mg L}^{-1}$ ) for 15 stations in Lake Alexandrina from the River Murray entrance to Clayton. Note that the Fell results were often below detection limit.

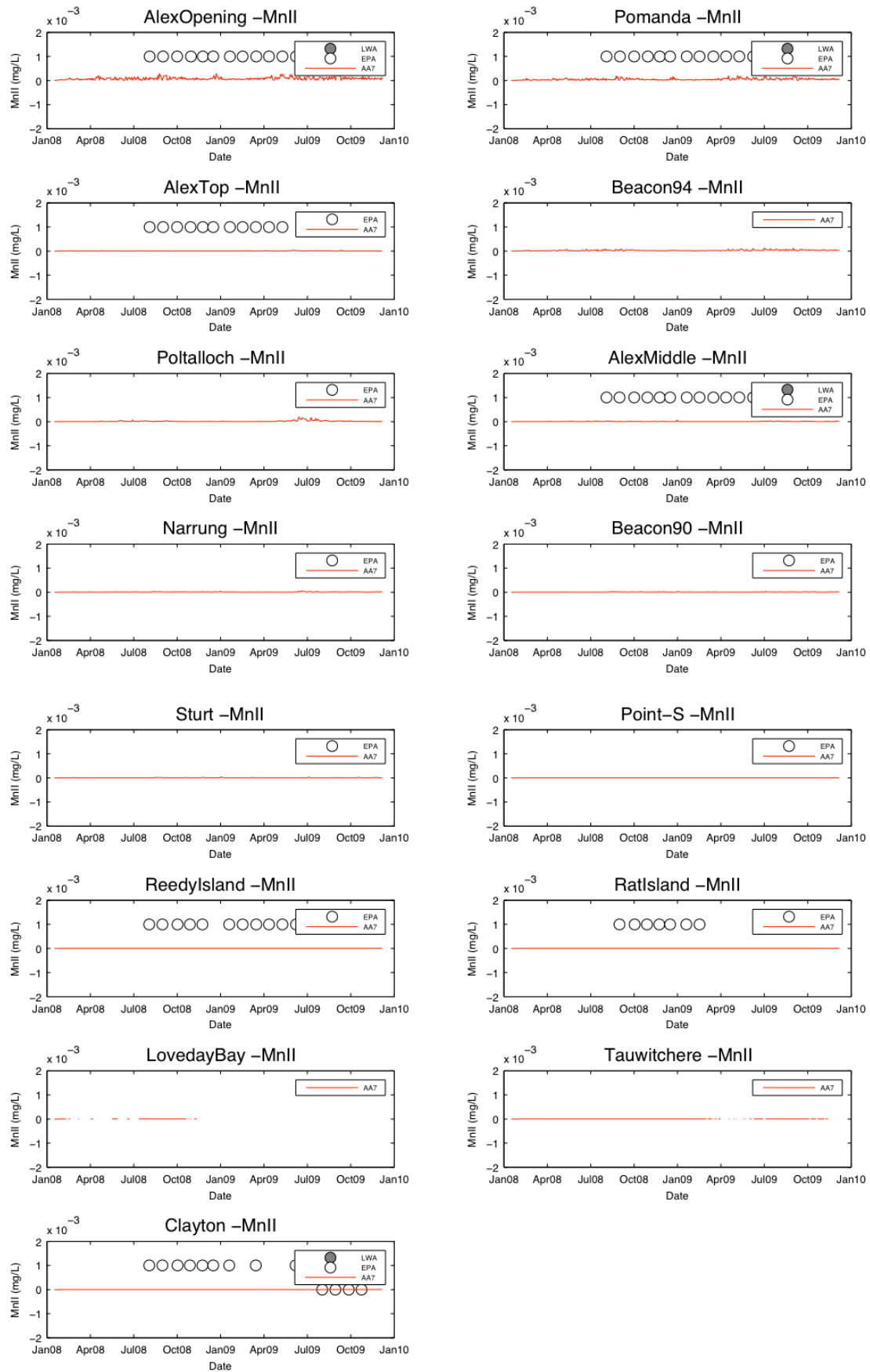


Figure 6.33: Comparison of modelled (Va) and measured (EPA) reduced manganese (MnII) data ( $\text{mg L}^{-1}$ ) for 15 stations in Lake Alexandrina from the River Murray entrance to Clayton. Note that the MnII results were mostly below detection limit.

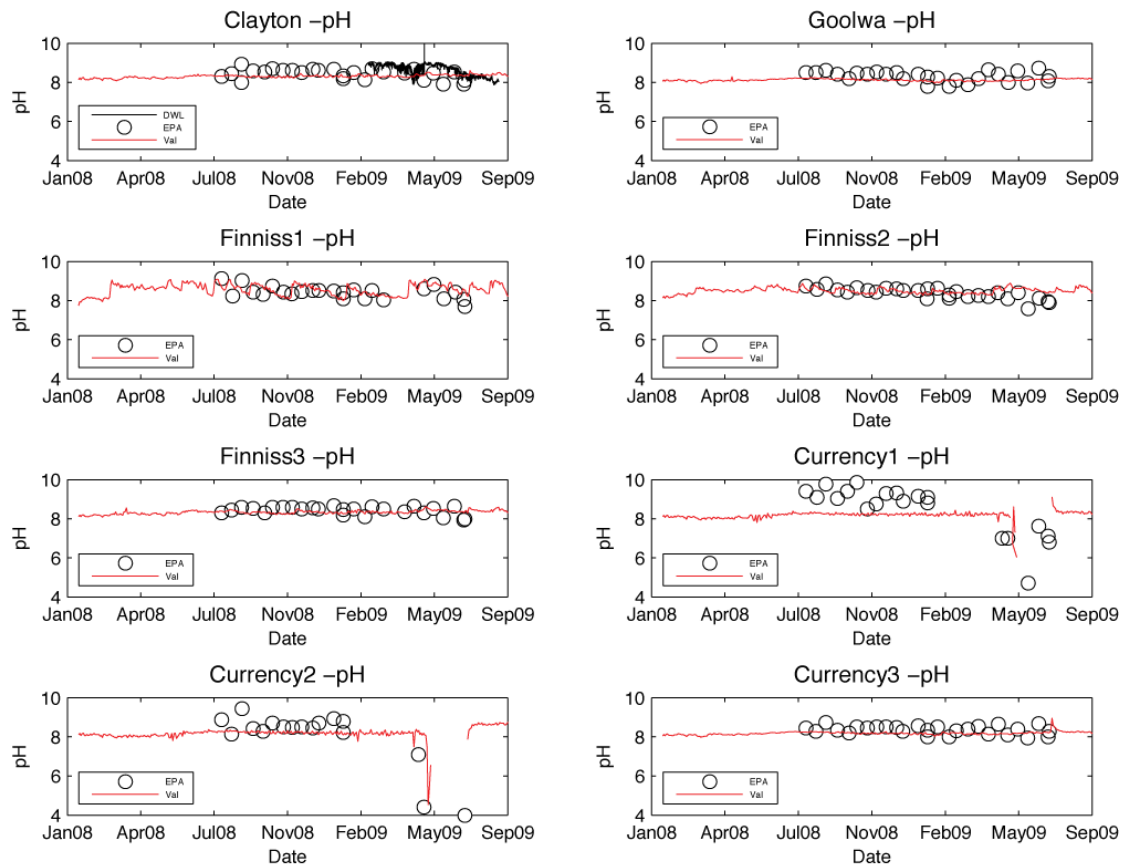


Figure 6.34: Comparison of modelled (Val) and measured (EPA & DFW) pH for 8 stations in Lake Alexandrina from within the Clayton to Goolwa sub-region. Note that this is modelled using the coarse Lake Alexandrina domain (AA) and the high resolution Currency Creek validation is presented in Section 6.3.

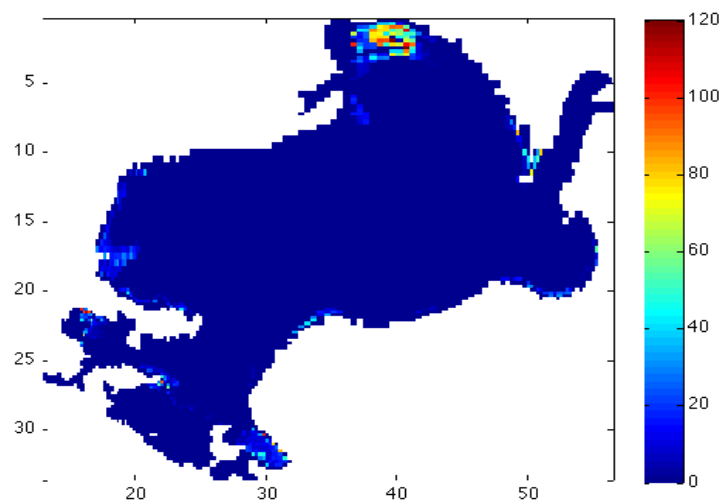


Figure 6.35a: Plot of modelled surface soil acidity ( $\text{mol H}^+ \text{m}^{-2}$ ) taken in Dec 2009. Spatial distribution qualitatively compares favourably with Fitzpatrick et al. (2010) TAA and surface soil pH maps.

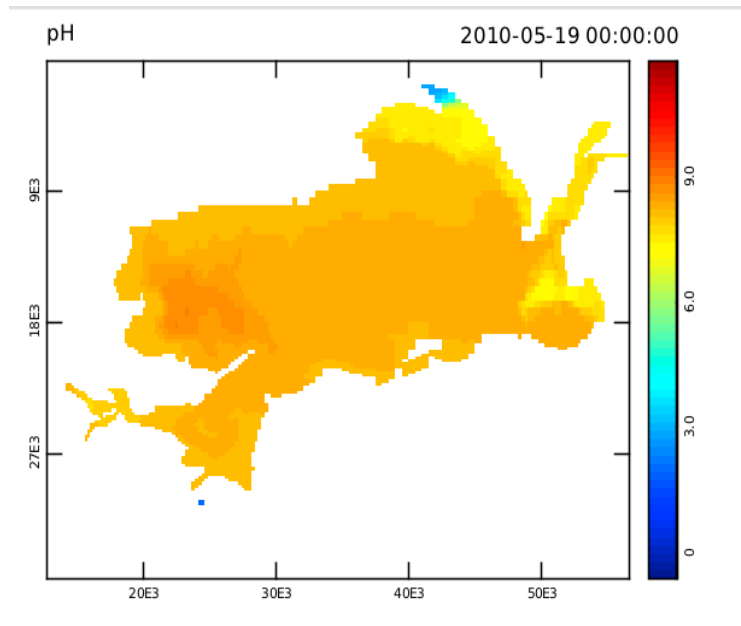


Figure 6.35b: Plot of modelled pH taken in May 2010. The water was observed to acidify (to  $\sim$ pH=2.5) in the northern region (Boggy Lake) in May 2010, one week after this predicted occurrence by the model. Note that this plot is from the continued drawdown scenario simulation that extended beyond the September 2009 simulations reported throughout this section and therefore has assumed flow and meteorological conditions for 8 months prior to this plot.

### **6.3 Lake Alexandrina (Clayton-Goolwa): validation (Jan 2008 – Sep 2009)**

For both Lake Albert and the main body of Lake Alexandrina outlined above, the validation to date includes assessment of performance of the model against the physical, chemical and biological parameters that are of interest around the lake and some small scale assessment of the acid sulfate soil model based on available soil data collected to date. The large AA (see Figure 6.3a) Lake Alexandrina domain shown in the above section did indicate a drying and general acidification of the Currency Creek region that occurred in 2009 but, since this was poorly resolved, it is not a sufficient validation of the model setup.

The Currency/Finniss high-resolution domain is therefore a critical component in this study for validating the acidification dynamics at a medium scale. The model simulations (labelled as 23f) is validated against available Department for Water (DFW) and Environment Protection Authority (EPA) routine data and strategically collected (CCF) water quality data collected by the EPA following acidification events.

#### **Hydrodynamics**

The water levels at the lower reaches are accurately predicted, however there was no water level data available for validation of the Currency pool depths once they became disconnected (Figure 6.36). The model did predict the disconnection of the upper and lower Currency tributary pools at about the right time, and the maintenance of connection in the Finniss tributary, so the predictions are considered at least qualitatively reasonable. The surface temperatures with the above configuration were well predicted throughout the simulation period (Figure 6.37) and compared well with both the EPA grab data and the real-time DFW temperature loggers. Some spatial variability was seen in the model data, particularly in Currency Creek after the pools began to form in early 2009. For salinity (plotted as electrical conductivity at 25°C, Figure 6.38), there is a notable horizontal gradient across the model domain that is generally captured by the model. There is also a significant increase in salinity across the domain during the 08/09 summer period that is captured generally by the model except in the upstream areas of the Currency Creek tributary. The very sharp salinity increase in the upper Currency Creek pool (during summer of 2008-09) is not seen in the model due to inflowing water from the inflowing boundary condition. Therefore, there is likely some error in applying the Currency flow measurements directly at the domain boundary (since they are measured upstream) and there is also potentially a appreciable groundwater contribution.

#### **Nutrients and Chl-a**

Dissolved Oxygen was highly variable, but the range was captured well by the model (Figure 6.39). The DOC level follows a noticeable seasonal trend (Figure 6.40) that is captured accurately by the model, although the concentration is under predicted at the upper Currency Creek station. NH<sub>4</sub> and NO<sub>3</sub> levels are low throughout the period and at or around the detection limit (Figure 6.41-6.42). The increase in NH<sub>4</sub> during mid 2009 in Finniss stations is captured by the model; this could be due to reintroducing anoxic conditions (NO<sub>3</sub>->NH<sub>4</sub>) or cation exchange as seen in some of the experiments. TN is accurately predicted and captures the large seasonal changes that occurred (Figure 6.43). PO<sub>4</sub> is well predicted and TP is predicted to have a similar trend as TN. A TP increase over summer is not seen as is for TN, indicating a P loss process that is not well accounted for in the model and could be related to adsorption processes (Figure 6.45). Total Chlorophyll-a (Figure 6.23) is predicted to be high by the model; comparison with the limited available data was reasonable. There is a strong seasonal trend of Chl-a increase and this follows the trend in temperature, with higher concentrations at the end of summer and low concentrations in winter.

#### **Lake Geochemistry**

The major ion (Ca, Na, Mg, Cl, SO<sub>4</sub>) concentrations in the main channel were predicted in line with observations, however the upstream Currency Creek (and to a lesser extent Finniss River) tributary stations showed significant deviations, particularly related to the sharp concentration increase over the early 2009 dry period. For the conservative ions (e.g. Na, Cl and Mg) the model does evaporate these ions of this period, but the model concentrations are less than the observed peak by approximately 30%. This could be due to errors in the predicted pool starting size, the lack of groundwater contribution in the model, or errors associated with the inflow boundary specification. For Ca and SO<sub>4</sub>, the errors are larger, likely due to the errors as outlined above, plus the lack of explicit contribution of these ions from the acid sulfate soil oxidation and acid neutralisation processes in the model. Additionally, addition of limestone to manage acidification was conducted

in the field but has not been considered in the model. For better resolution of these dynamics it is recommended the model be extended to account for key ions in the acid sulfate soil leachate, in addition to acidity, in order to study the impact of the leachate on surface water quality in more detail.

The acidity flux from the model is small until the first rains of 2009, at which point both the Currency Creek tributary pools go acidic, in May 2009 (Figure 6.55). The model predicts the timing and extent of the acidity well. There are however some parts of the domain that are also predicted to experience acid pulses that are not seen in the observed record. These are only short lived and most likely due to erroneous specification of soil textural properties near the domain perimeter. It also appears that there is some slight disconnection in the Finniss tributary from the main channel that did not occur in reality; connectivity would have served to flush any local acidity flux away and prevent local acidification. The DIC concentrations (Figure 6.56) show some unexpected concentrations. They do drop during acidification but then quickly respond upon refilling, more so than in the observed data. The concentrations are also substantially over-predicted in the upstream sites; this appears to be due to very high alkalinity concentrations used when specifying DIC in the inflows. We therefore recommend further work be conducted to obtain comprehensive model input data and improve the alkalinity and geochemical predictions made by the model in this area.

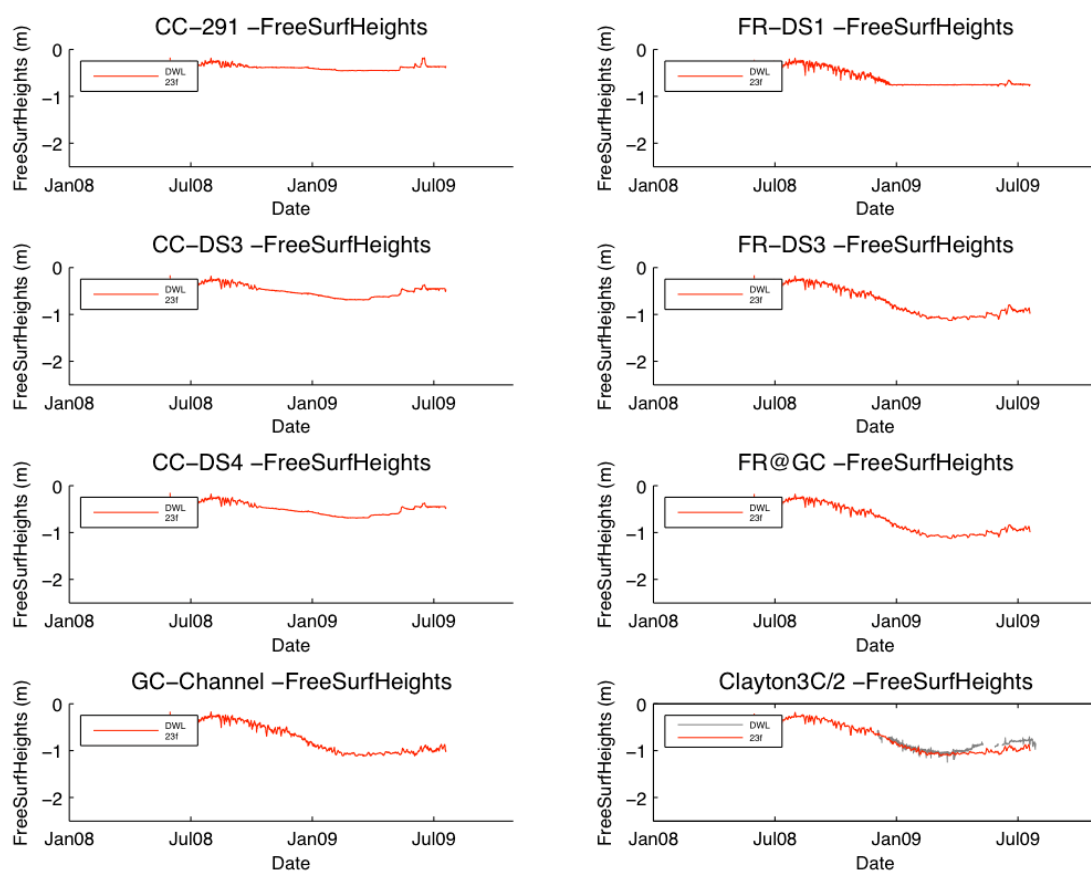


Figure 6.36: Comparison of modelled (23f) and measured (LWA, EPA & CCF) water level for 8 stations between Clayton and Goolwa (refer to Figure 5.10 for locations).

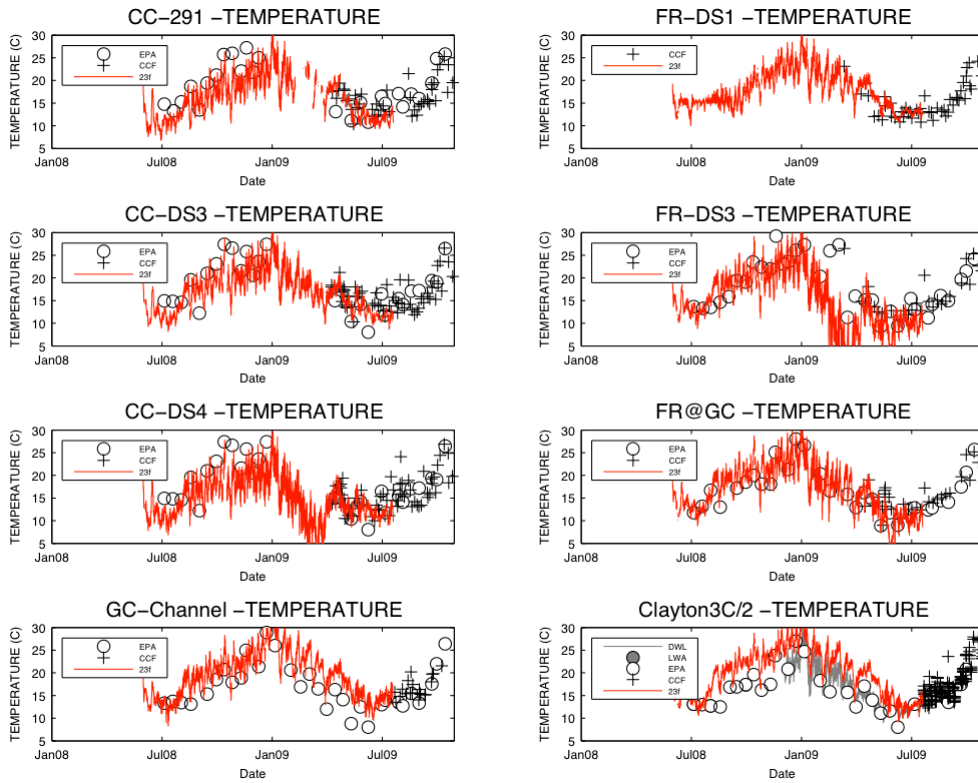


Figure 6.37: Comparison of modelled (23f) and measured (LWA, EPA & CCF) temperature ( $^{\circ}\text{C}$ ) for 8 stations between Clayton and Goolwa (refer to Figure 5.10 for locations).

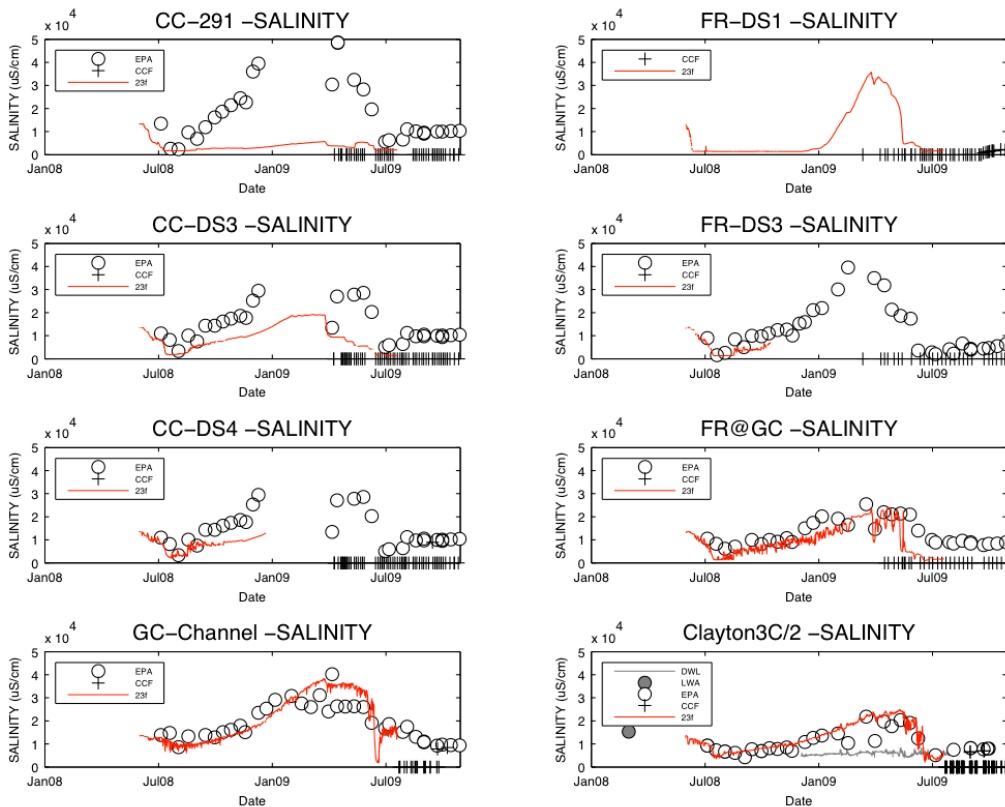


Figure 6.38: Comparison of modelled (23f) and measured (LWA, EPA & CCF) salinity (as EC,  $\mu\text{Scm}^{-1}$ ) for 8 stations between Clayton and Goolwa (refer to Figure 5.10 for locations).

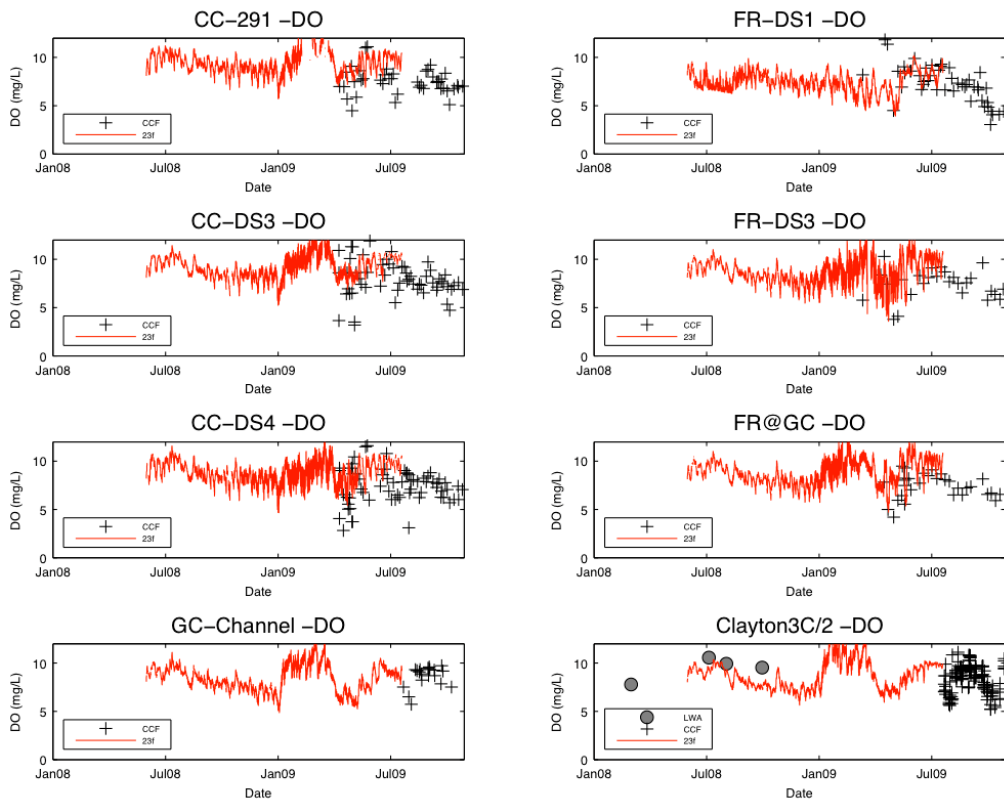


Figure 6.39: Comparison of modelled (23f) and measured (LWA, EPA & CCF) dissolved oxygen (DO, mg L<sup>-1</sup>) for 8 stations between Clayton and Goolwa (refer to Figure 5.10 for locations).

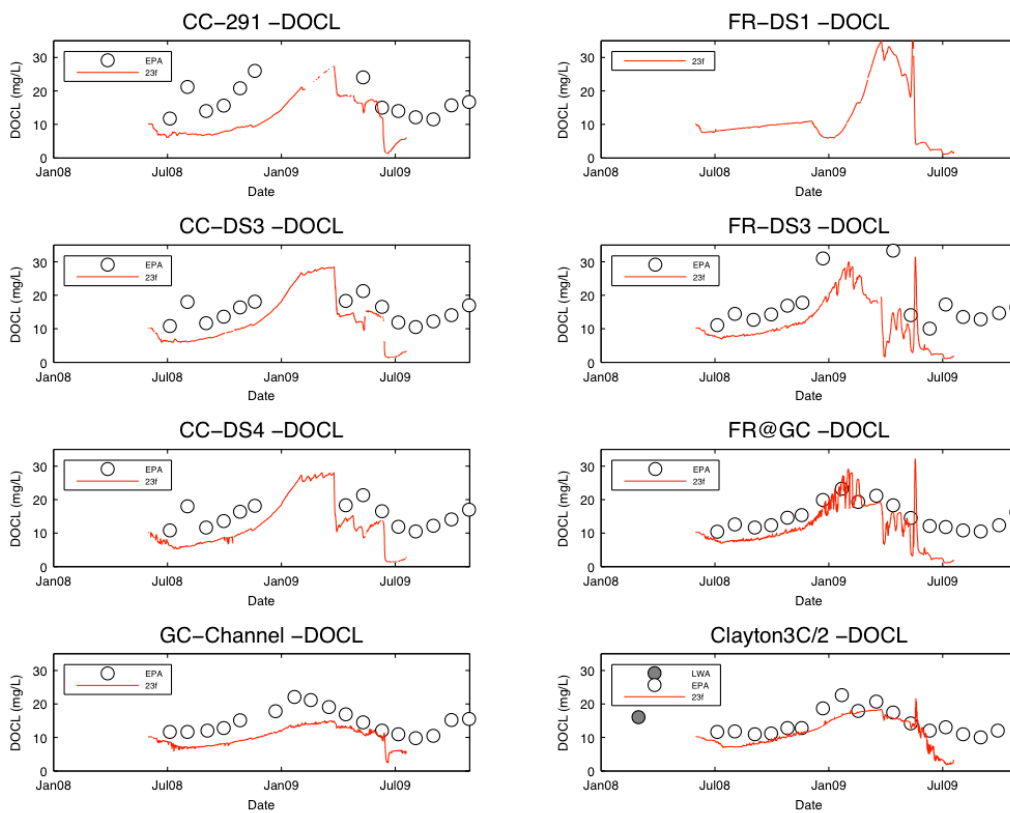


Figure 6.40: Comparison of modelled (23f) and measured (LWA, EPA & CCF) dissolved organic carbon (DOC, mg L<sup>-1</sup>) for 8 stations between Clayton and Goolwa (refer to Figure 5.10 for locations).

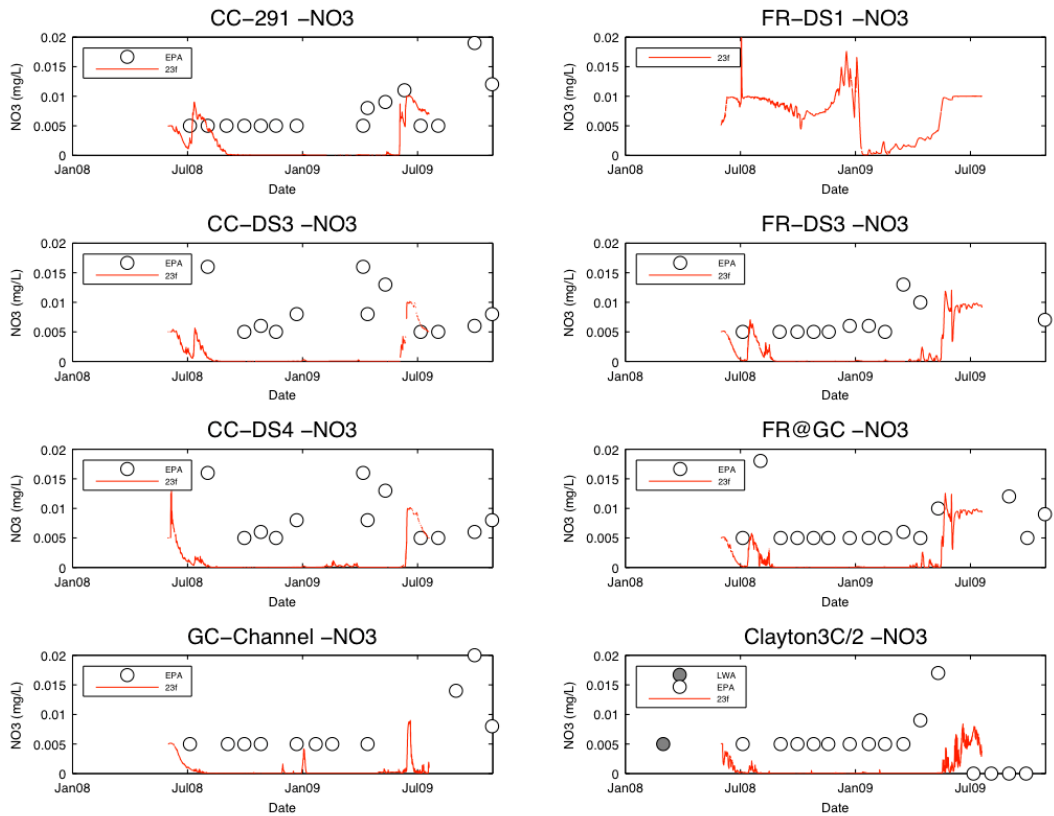


Figure 6.41: Comparison of modelled (23f) and measured (LWA, EPA & CCF) NO<sub>3</sub>-N (NO<sub>3</sub>, mg L<sup>-1</sup>) for 8 stations between Clayton and Goolwa (refer to Figure 5.10 for locations).

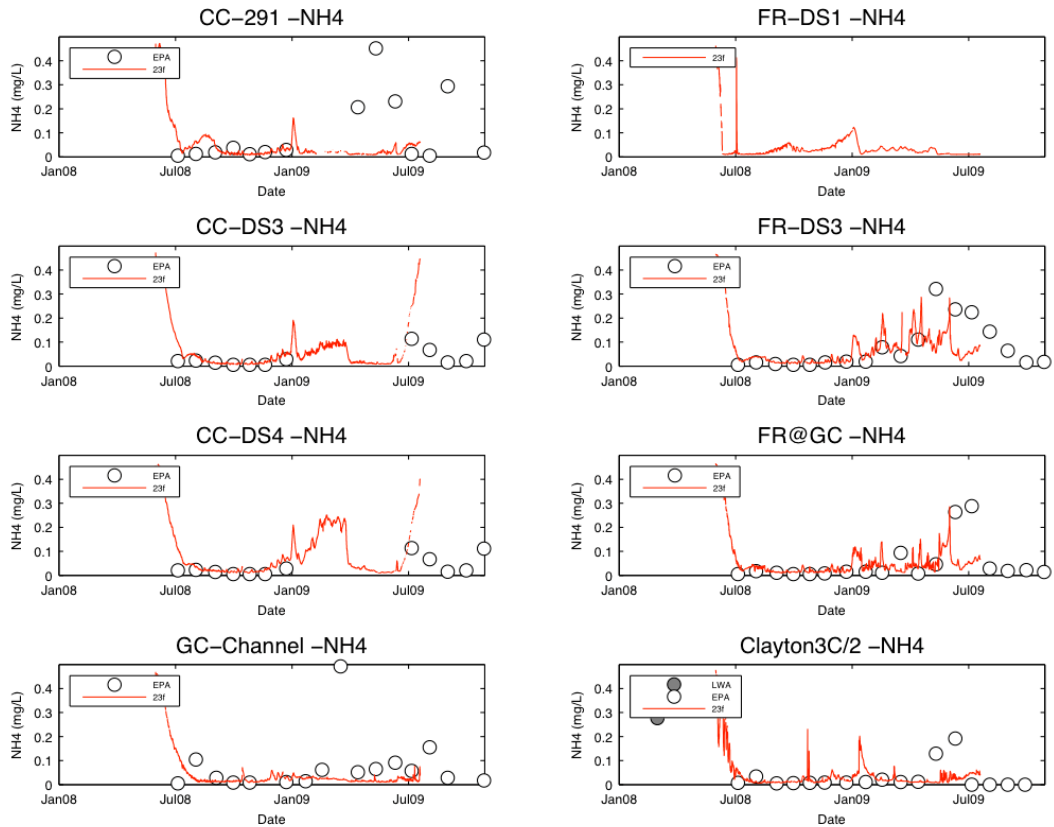


Figure 6.42: Comparison of modelled (23f) and measured (LWA, EPA & CCF) NH<sub>4</sub>-N (NH<sub>4</sub>, mg L<sup>-1</sup>) for 8 stations between Clayton and Goolwa (refer to Figure 5.12 for locations).

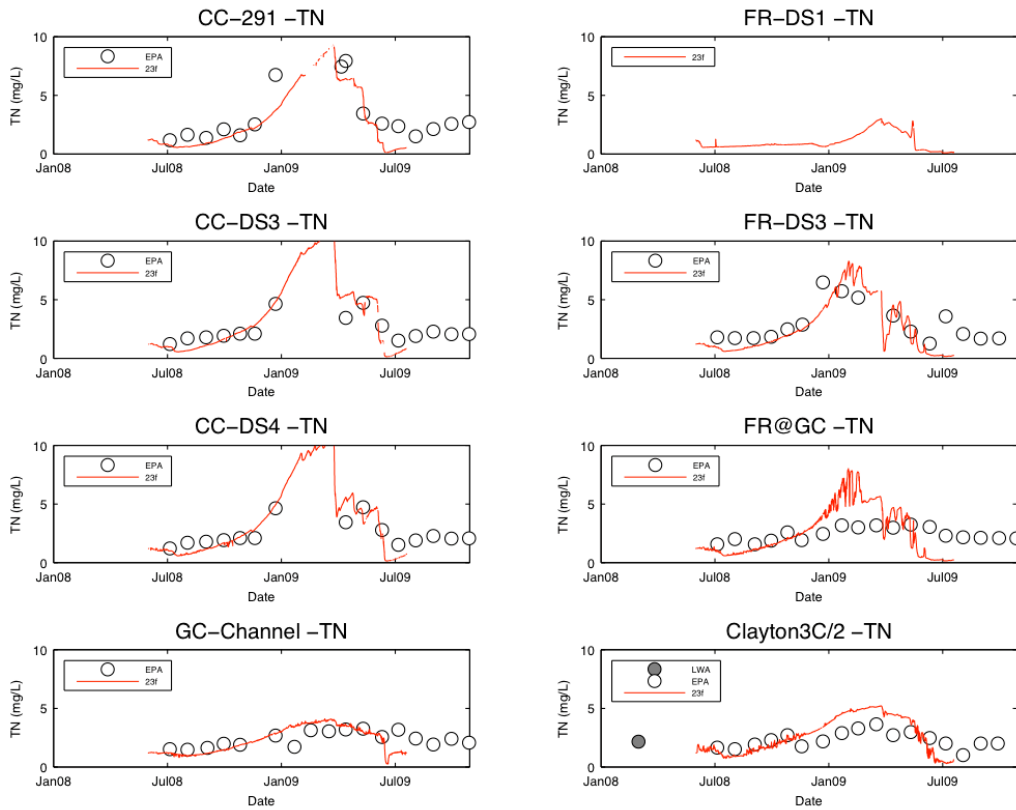


Figure 6.43: Comparison of modelled (23f) and measured (LWA, EPA & CCF) total nitrogen (TN, mg L<sup>-1</sup>) for 8 stations between Clayton and Goolwa (refer to Figure 5.12 for locations).

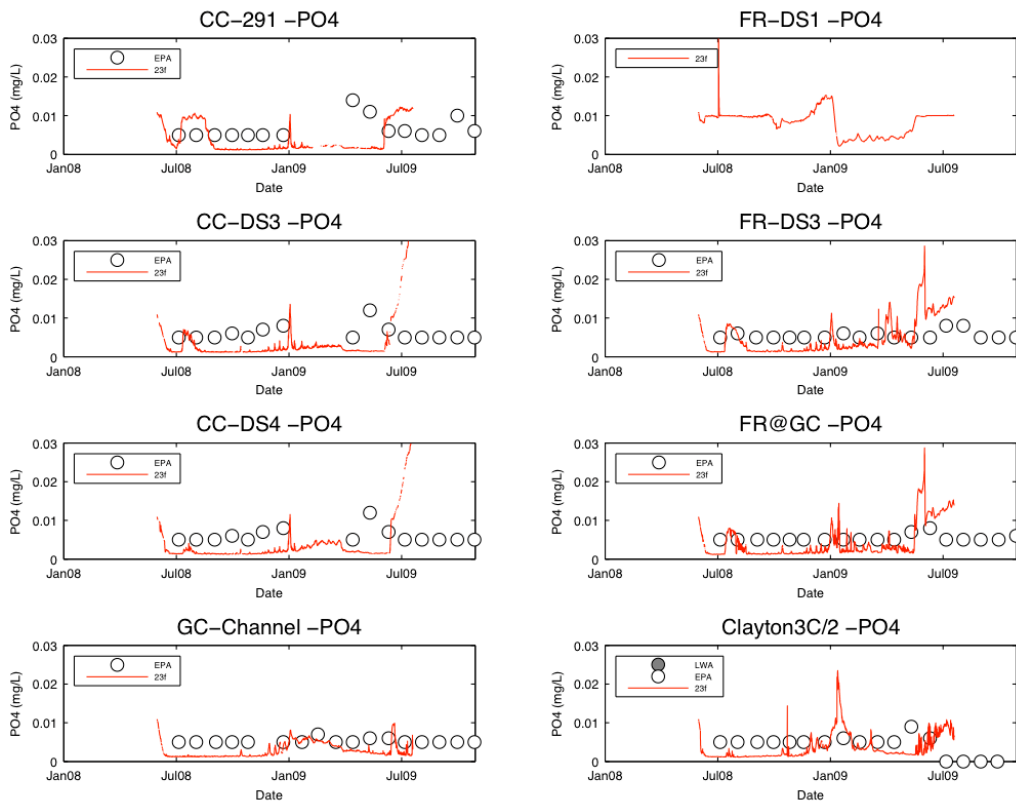


Figure 6.44: Comparison of modelled (23f) and measured (LWA, EPA & CCF) filterable reactive phosphorus (PO<sub>4</sub>, mg L<sup>-1</sup>) for 8 stations between Clayton and Goolwa (refer to Figure 5.12 for locations).

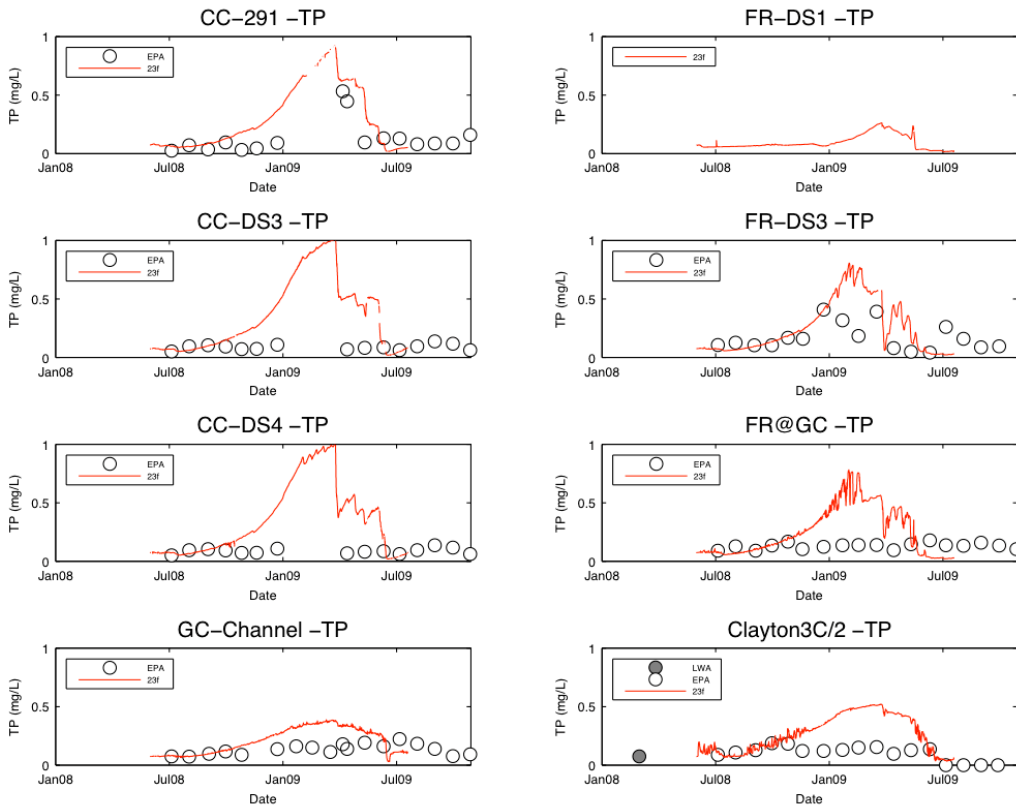


Figure 6.45: Comparison of modelled (23f) and measured (LWA, EPA & CCF) total phosphorus (TP, mg L<sup>-1</sup>) for 8 stations between Clayton and Goolwa (refer to Figure 5.12 for locations).

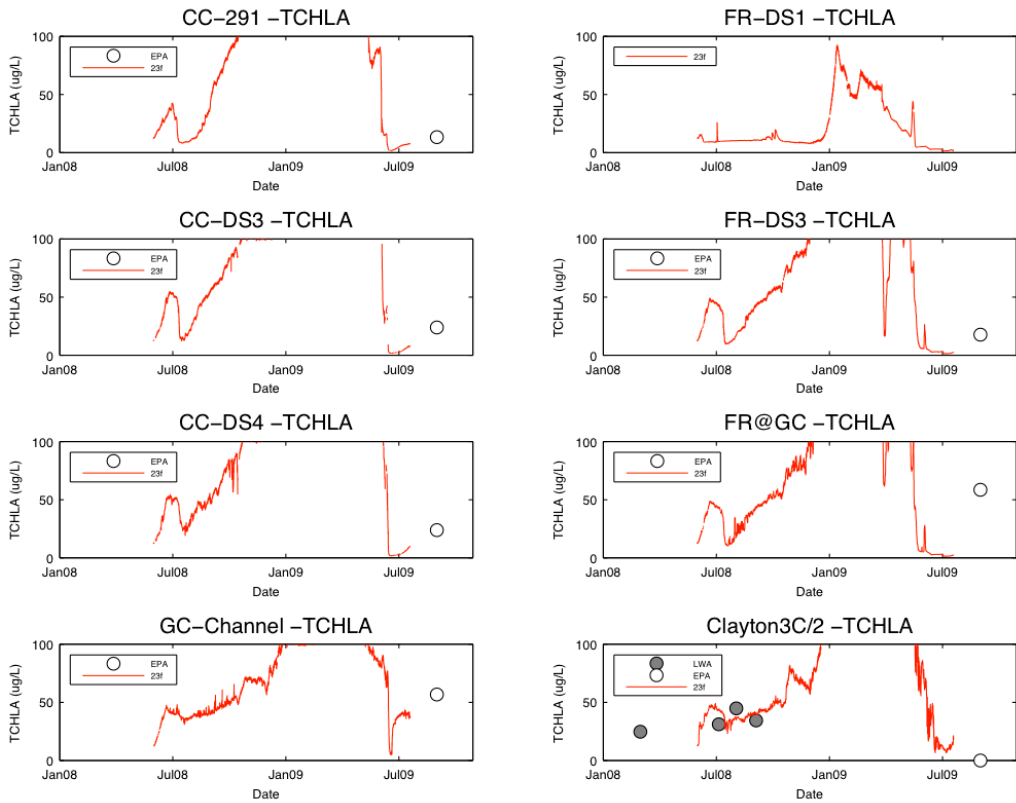


Figure 6.46: Comparison of modelled (23f) and measured (LWA, EPA & CCF) total chlorophyll-a (TCHLA, µg chl-a L<sup>-1</sup>) for 8 stations between Clayton and Goolwa (refer to Figure 5.12 for locations).

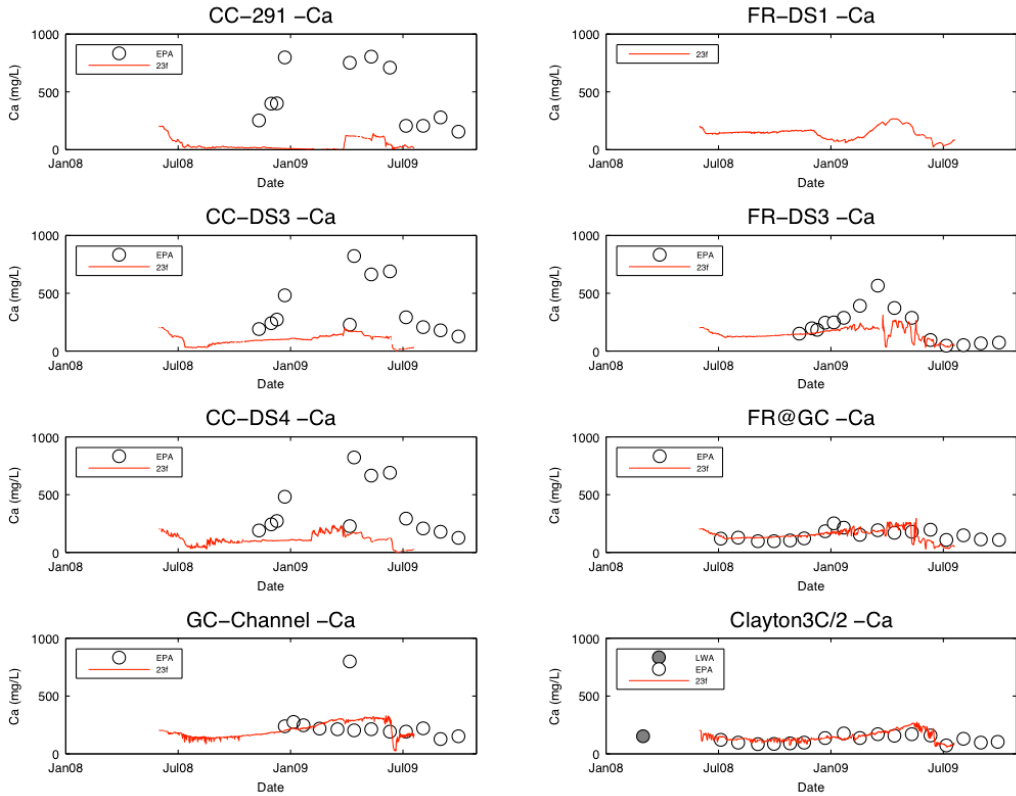


Figure 6.47: Comparison of modelled (23f) and measured (LWA, EPA & CCF) Ca ( $\text{mg L}^{-1}$ ) for 8 stations between Clayton and Goolwa (refer to Figure 5.12 for locations).

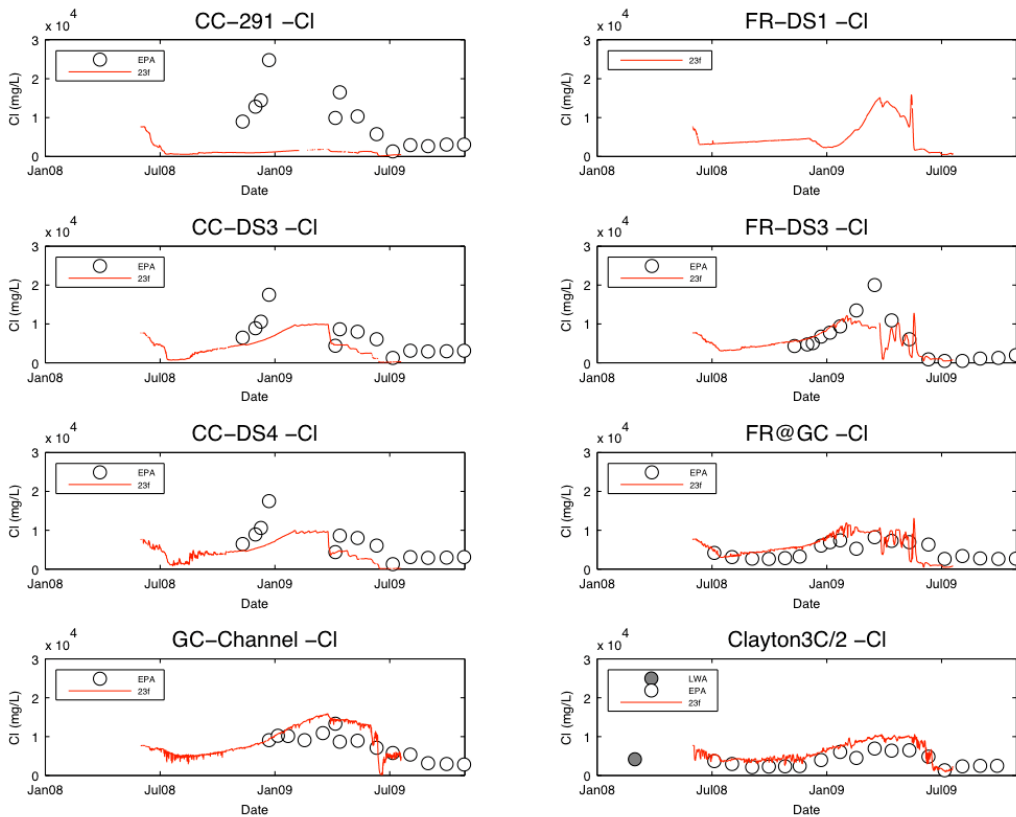


Figure 6.48: Comparison of modelled (23f) and measured (LWA, EPA & CCF) Cl ( $\text{mg L}^{-1}$ ) for 8 stations between Clayton and Goolwa (refer to Figure 5.12 for locations).

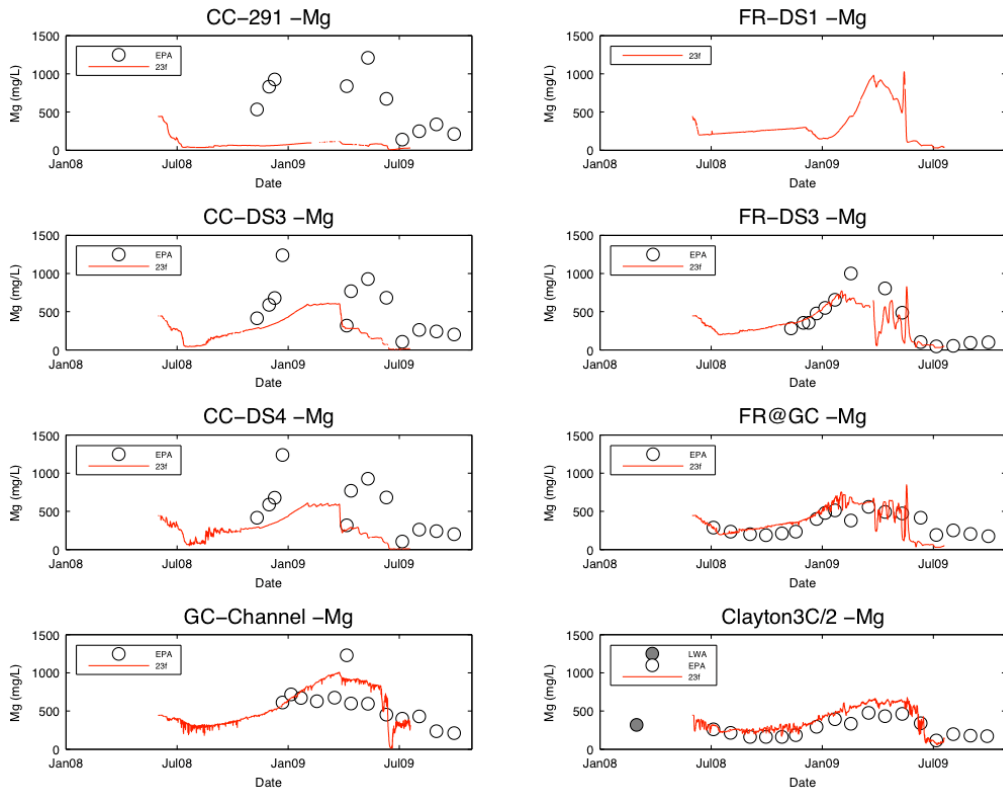


Figure 6.49: Comparison of modelled (23f) and measured (LWA, EPA & CCF) Mg ( $\text{mg L}^{-1}$ ) for 8 stations between Clayton and Goolwa (refer to Figure 5.12 for locations).

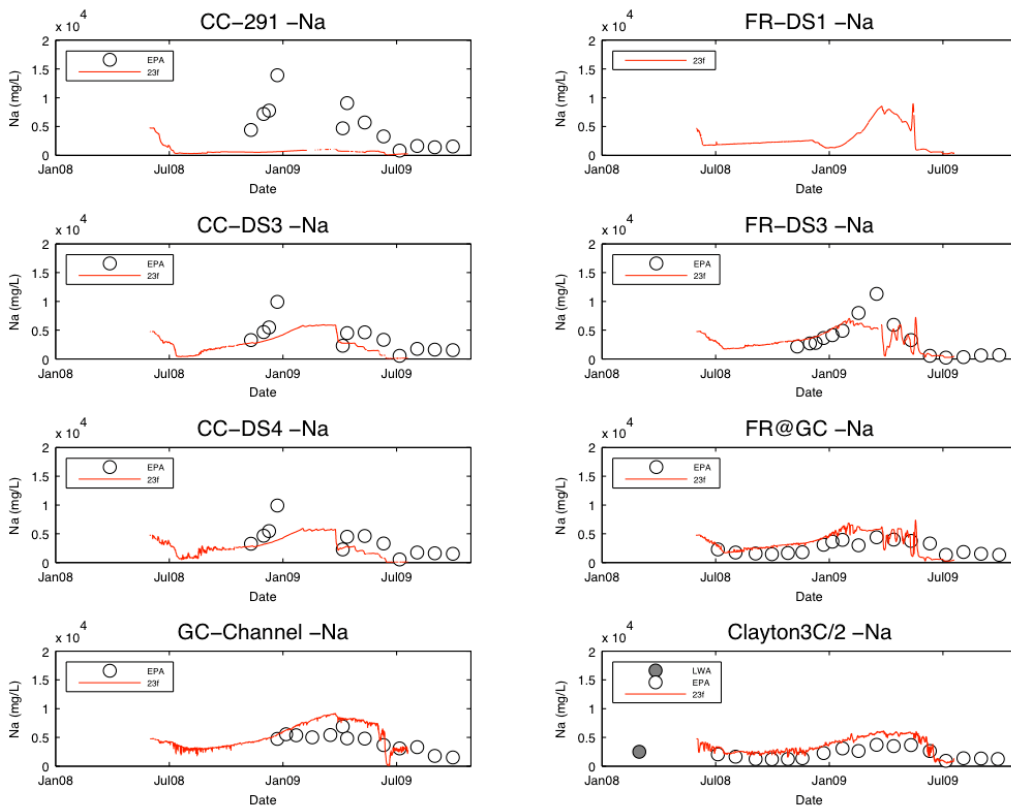


Figure 6.50: Comparison of modelled (23f) and measured (LWA, EPA & CCF) Na ( $\text{mg L}^{-1}$ ) for 8 stations between Clayton and Goolwa (refer to Figure 5.12 for locations).

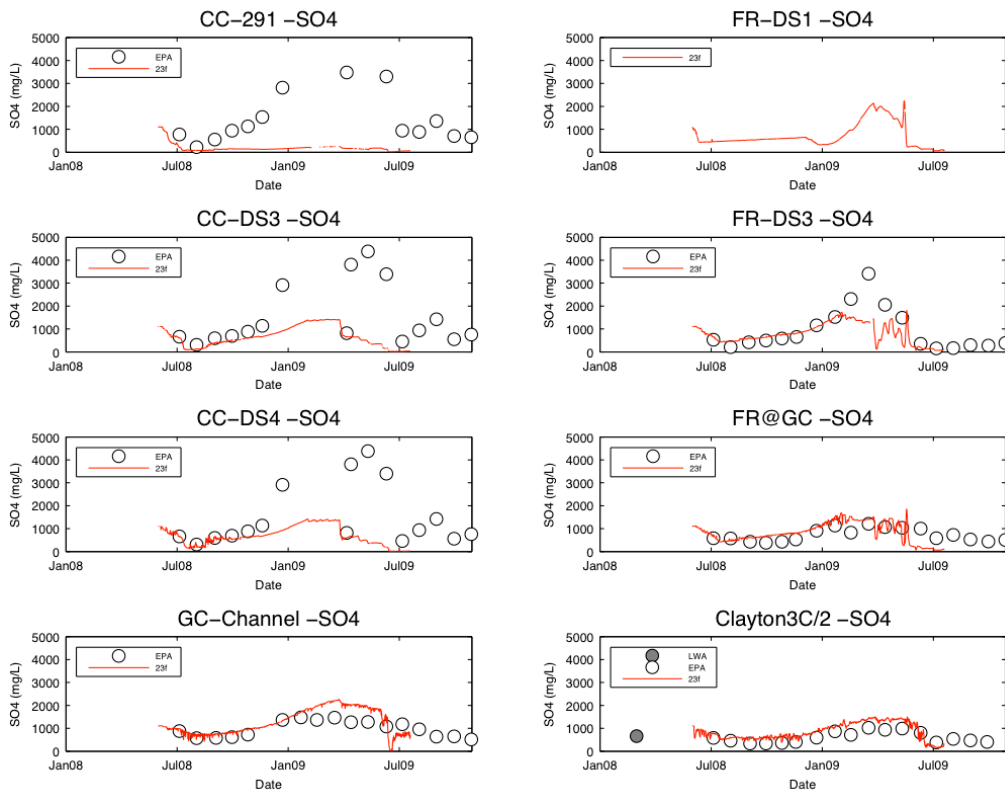


Figure 6.51: Comparison of modelled (23f) and measured (LWA, EPA & CCF) SO<sub>4</sub> (mg L<sup>-1</sup>) for 8 stations between Clayton and Goolwa (refer to Figure 5.12 for locations).

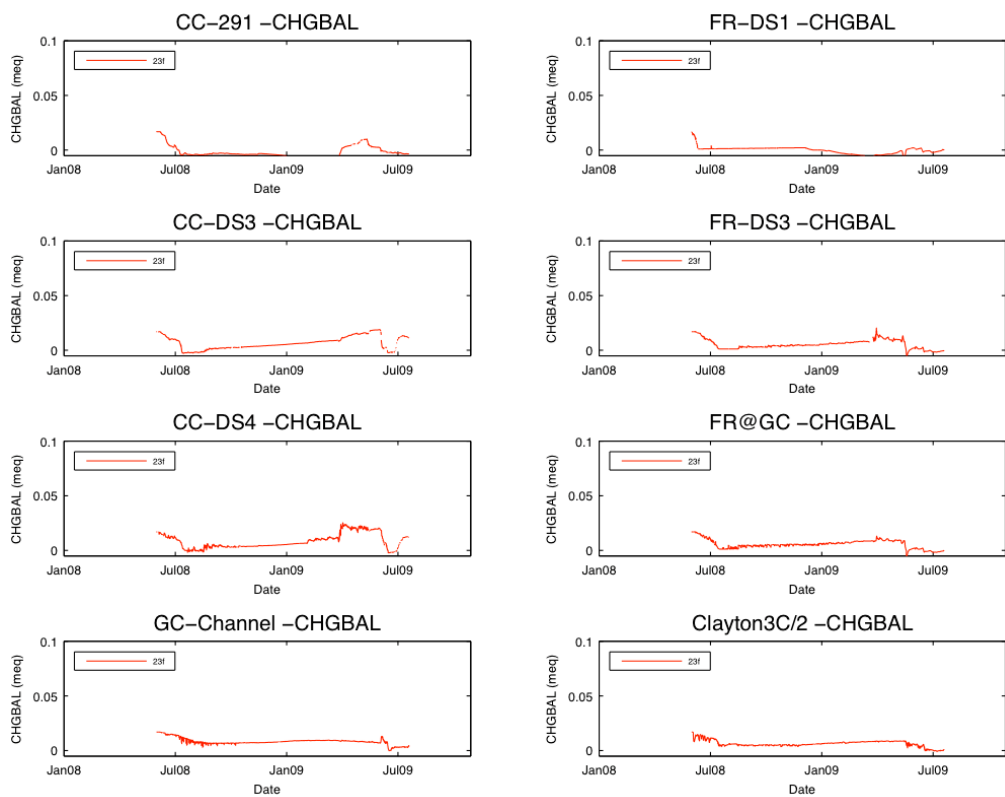


Figure 6.52: Comparison of modelled (23f) and measured (LWA, EPA & CCF) CHGBAL (meq) for 8 stations between Clayton and Goolwa (refer to Figure 5.102 for locations).

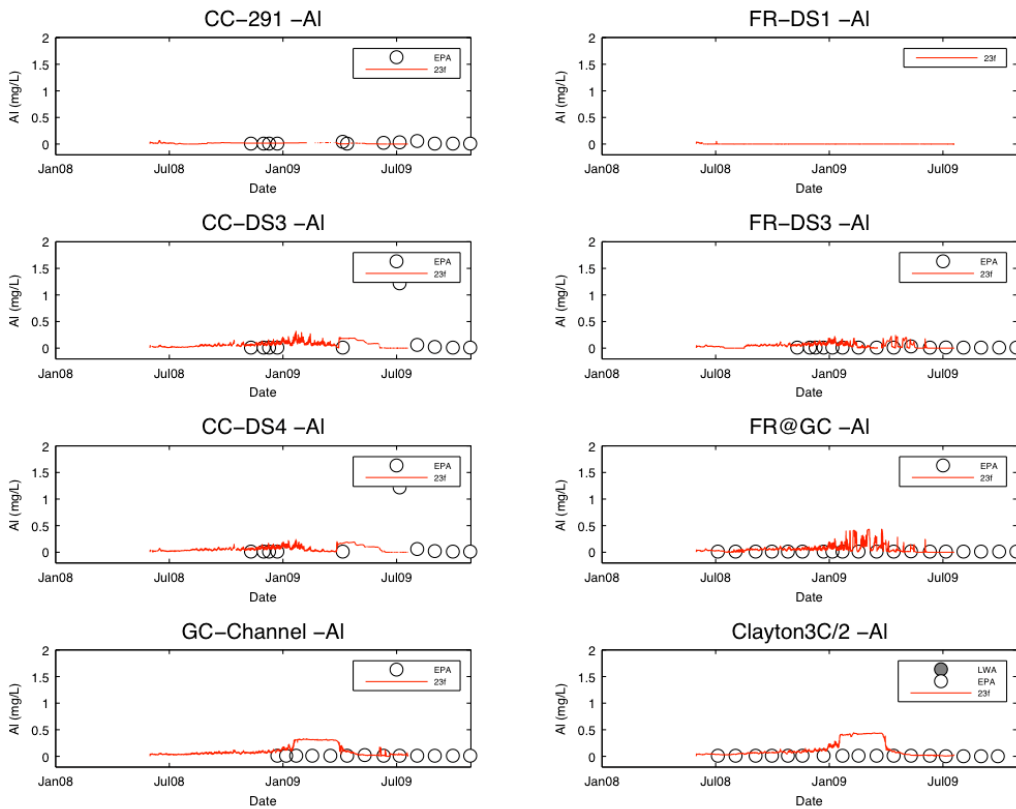


Figure 6.53: Comparison of modelled (23f) and measured (LWA, EPA & CCF) Al ( $\text{mg L}^{-1}$ ) for 8 stations between Clayton and Goolwa (refer to Figure 5.12 for locations).

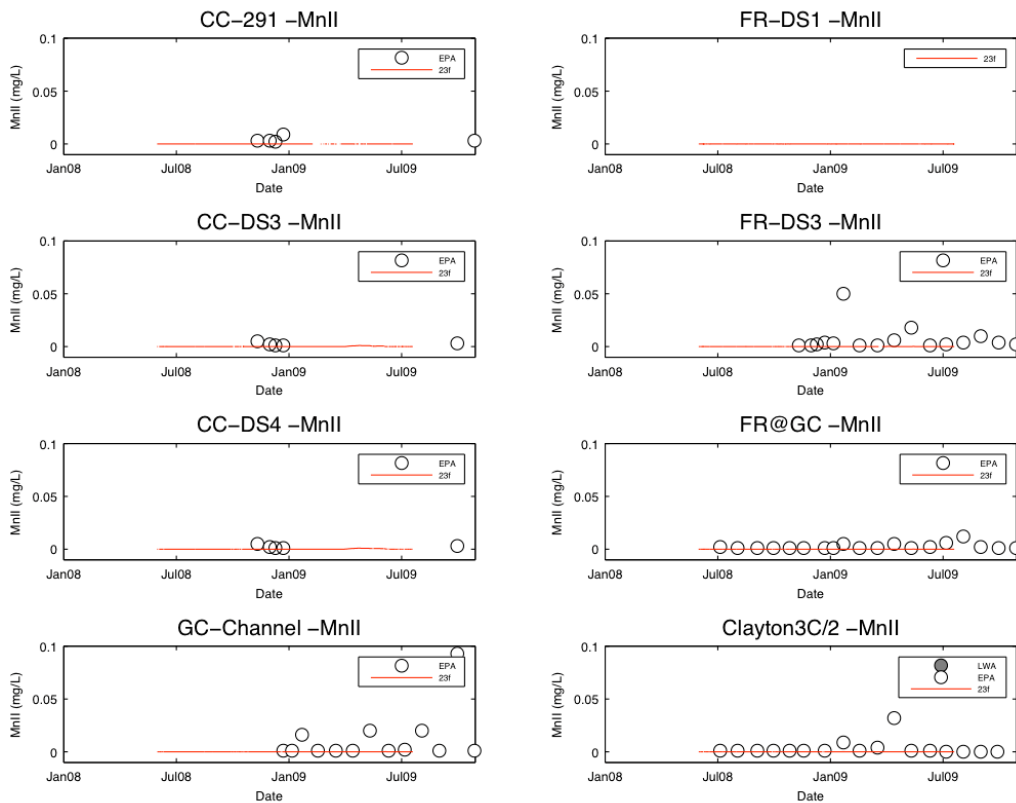


Figure 6.54: Comparison of modelled (23f) and measured (LWA, EPA & CCF) Mn ( $\text{mg L}^{-1}$ ) for 8 stations between Clayton and Goolwa (refer to Figure 5.12 for locations).

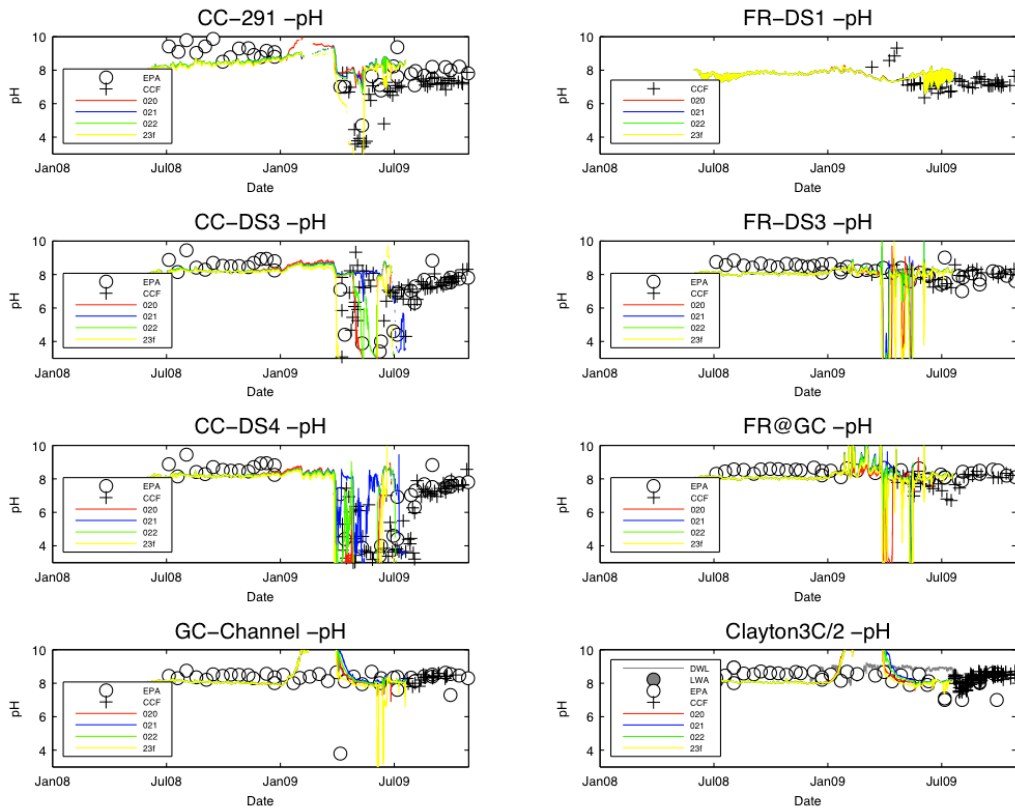


Figure 6.55: Comparison of modelled (23f) and measured (LWA, EPA & CCF) pH (-) for 8 stations between Clayton and Goolwa (refer to Figure 5.12 for locations).

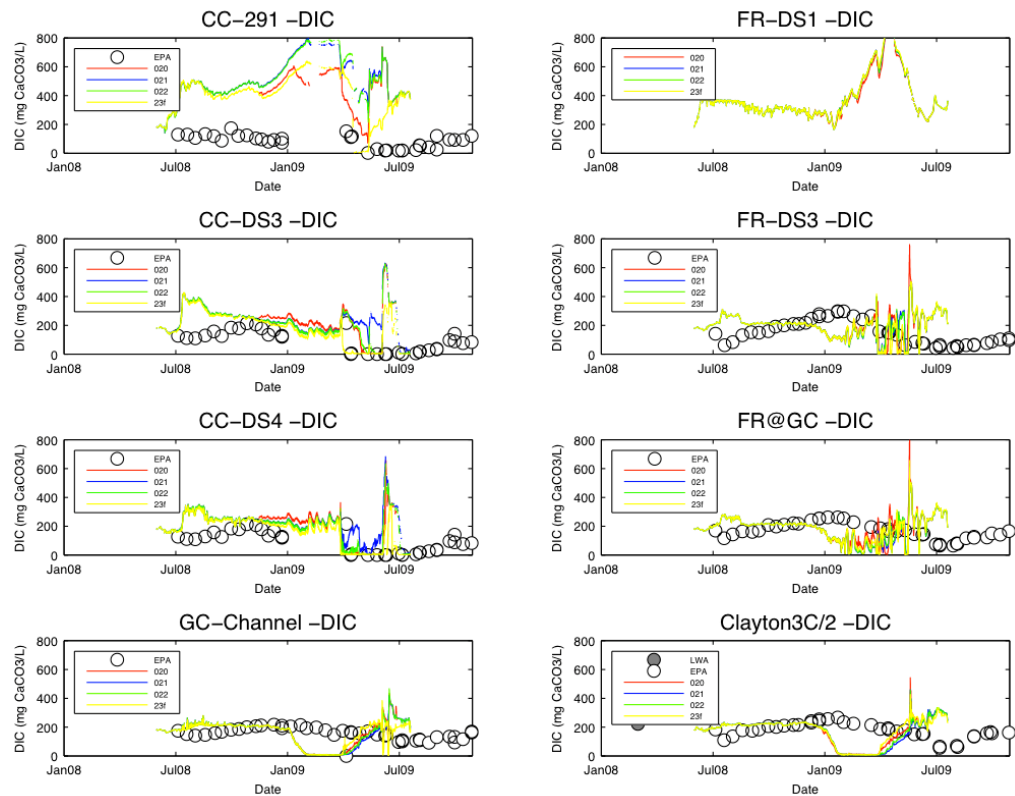


Figure 6.56: Comparison of modelled (23f) and measured (LWA, EPA & CCF) DIC for 8 stations between Clayton and Goolwa (refer to Figure 5.12 for locations).

## Soil Dynamics

A soil column profile predicted by the model for a representative boundary cell in the lower Currency Creek area illustrates the evolution of soil properties predicted over time (Figure 6.57). The depth of the soil profile here drains to approximately 50-70cm below the surface by mid 2009. This result is supported by the values recorded in upper and lower Currency Creek at this time (Earth Systems, 2010), although the measurements did indicate the water table dropped deeper than this at the end of the summer period. The model predicts that the PASS initially present in the top 20-30 cm is mostly oxidised over the course of the year (seen as PASS declining over time), but the pyrite deeper in the soil profile remains mostly un-oxidised due to the capillary rise above the water table keeping moisture levels relatively high for 20-30cm above the water table. This is qualitatively consistent with observations to date, and more work is recommended to study this in more detail.

Spatial plots of pH, DIC, water table depth and soil properties (Figure 6.58-6.62) also illustrate the variability across the domain and how it evolved during the simulation (panels indicated consecutive progression of around 3 months). The plots indicating the water table depth (PHREATIC) show the area of exposed sediment and the amount of soil material that has been exposed to oxygen. Despite the large area of exposed material and high concentrations of sulfides, the areas of acidic groundwater are patchy and develop in response to rainfall; the patterns that manifest are a result of the different values of soil type, sulfide concentration and ANC concentrations. The areas showing acidity in the saturated zone are also a smaller subset of the areas that show acidity in the unsaturated zone. The area between the main Goolwa channel and the Currency tributary is a key area where acidification develops, and areas adjacent to the two Currency Creek pools also generate a substantial amount of acidity.

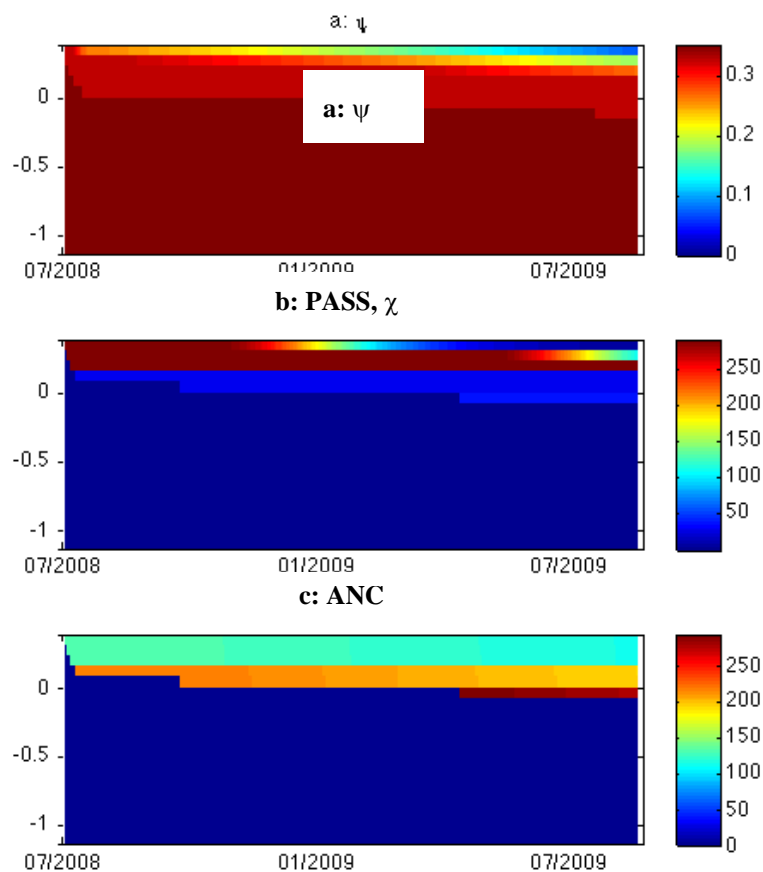


Figure 6.57: Soil profile evolution over the simulation period (vertical scale is depth, m AHD), showing a) soil moisture content, b) PASS concentration ( $\text{mol H}^+ \text{kg}^{-1}$ ) and c) ANC ( $\text{mol H}^+ \text{kg}^{-1}$ ) evolution.

The model also outputs an integrated time-series of the acid sulfate soil processes (Figure 6.63) to allow a large-scale overview of the dominant drivers. The results highlight the large accumulation of acidity in the unsaturated zone (as seen in the of sandy regions of the map plots, Figure 6.60), which slowly moves into in the saturated zone. There is a seasonal pattern of acidity production and subsequent neutralisation by ANC, however the rate of neutralisation is about 1/3 of the oxidation rate. As indicated in the SZAASS map (Figure 6.61) only small areas of the groundwater are acidic; this is reflected in the model spatial integration that shows a net negative acidity (i.e., a positive alkalinity) store even following acidification of the Currency Creek pools. Percolation on May/June however did generate a substantial downward acidity flux towards the water table. Interestingly, although the groundwater remained net alkaline, the seepage flux by Jun 2009 was acidic; i.e., those cells mostly contributing towards lateral flow towards the waterbody were net acidic, implying that the majority of groundwater was not acidic and provides a large reservoir of alkalinity, but is not connected to the surface water processes. The dominant driver however was the flux that occurred due to saturation excess, ponding and throughflow occurring above the water table. This plot indicates that while the smaller rainfall events contribute to a vertical redistribution of acidity, the intense rainfall events that occurred (e.g., in May 2009) reach a threshold above the soils capacity and this results in water collecting acidity and transporting it laterally to the Currency Creek pool. Rewetting of acidic sediment also generated a notable flux overall, though  $\text{SO}_4$  reduction by inundated lake sediment was of a similar magnitude.

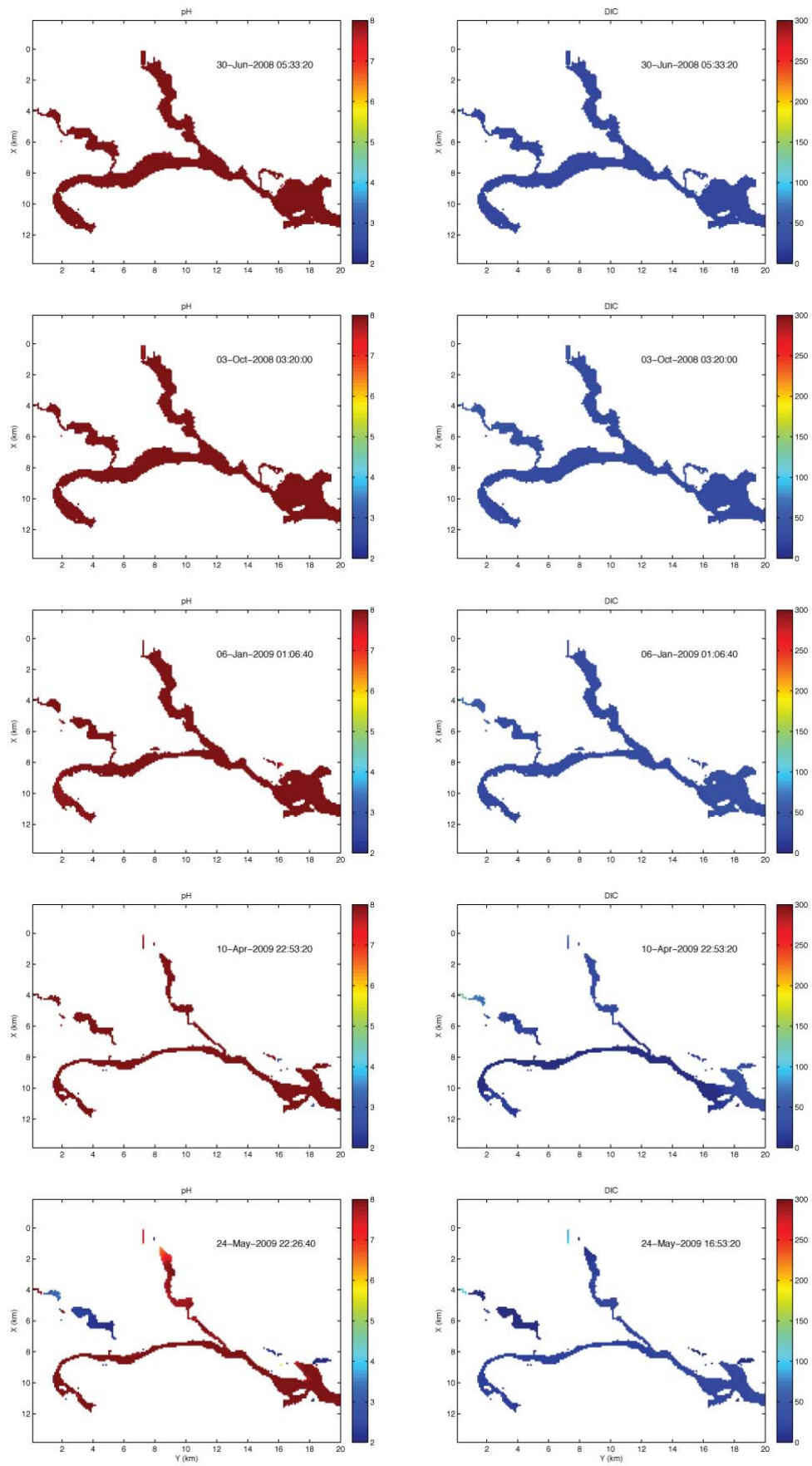


Figure 6.58: Plots of pH and dissolved carbonate alkalinity (DIC, mg C L<sup>-1</sup>) at intervals through 2008-2009.

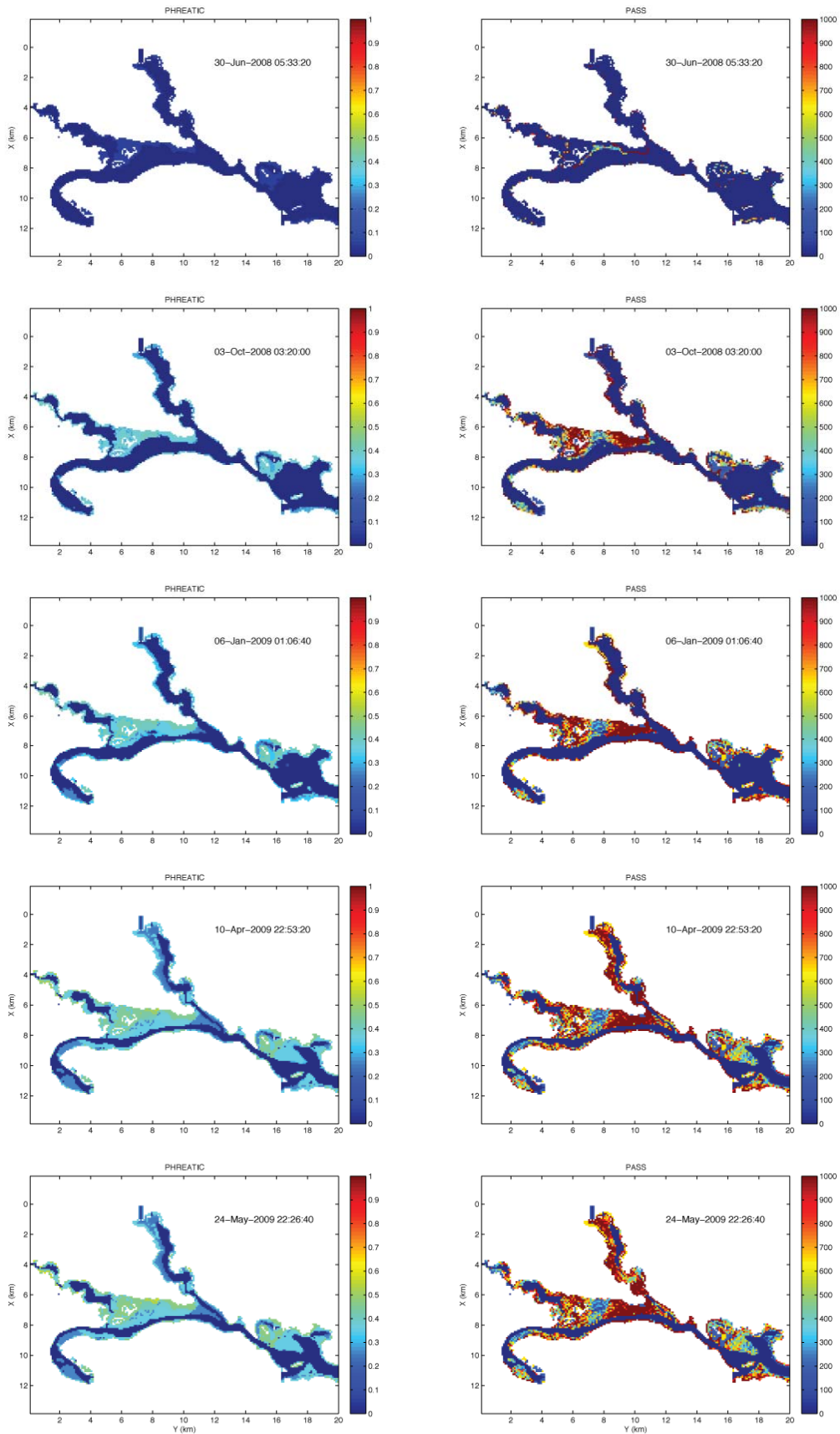


Figure 6.59: Plots of water table depth (PHREATIC, m) and exposed PASS ( $\text{mol H}^+ [10000\text{m}^2]^{-1}$ ) at intervals through 2008-2009.

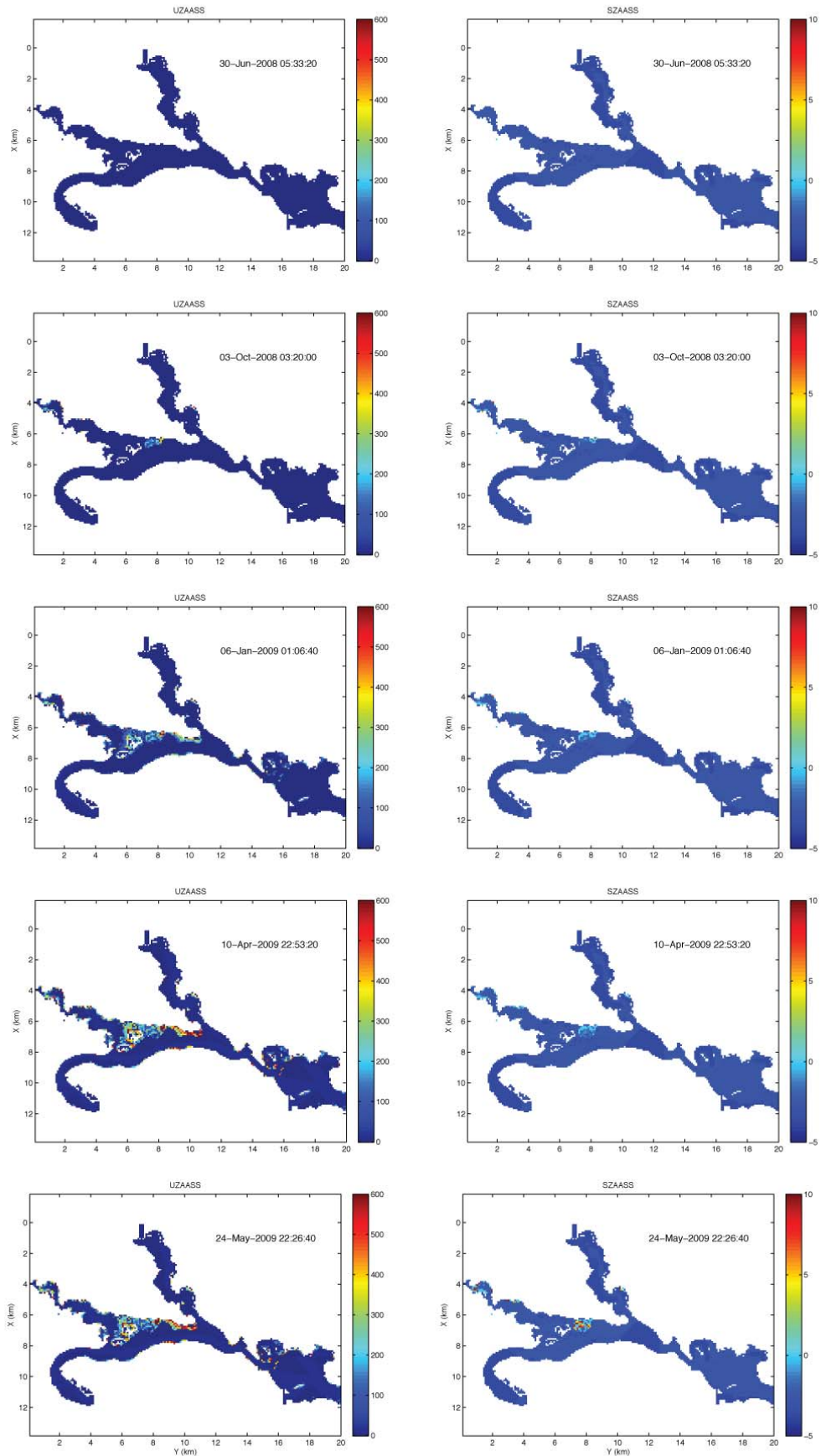


Figure 6.60: UZAASS (mol H<sup>+</sup> [10000m<sup>2</sup>]<sup>-1</sup>) and SZAASS (mol H<sup>+</sup> [10000m<sup>2</sup>]<sup>-1</sup>) at intervals through 2008-2009.

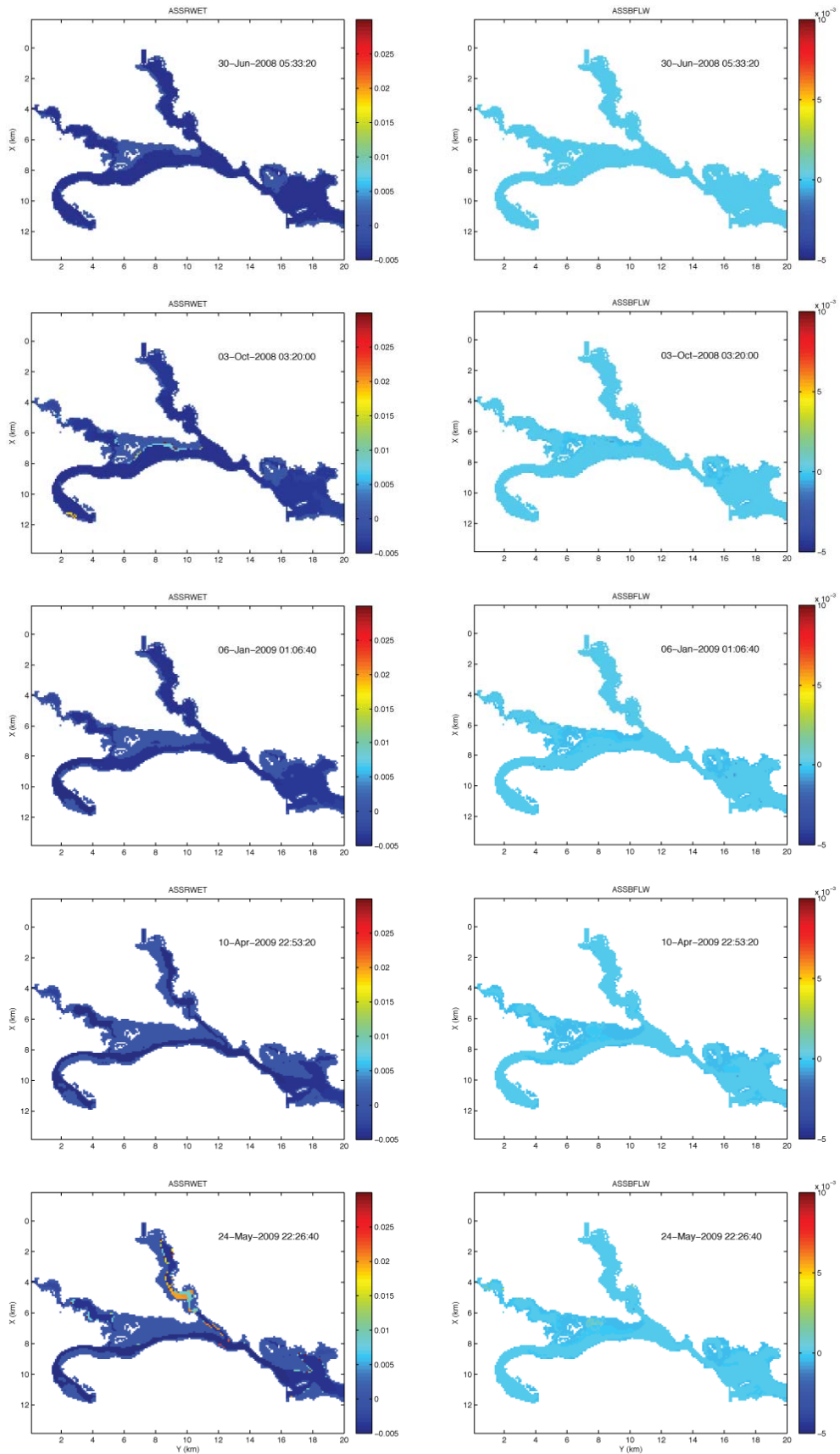


Figure 6.61: Plots of acidity flux rate during inundation (ASSRWET, mol H<sup>+</sup> m<sup>-2</sup> day<sup>-1</sup>; negative implies alkalinity) and acidity flux rate via seepage (ASSBFLW, mol H<sup>+</sup> day<sup>-1</sup>) at intervals through 2008-2009.

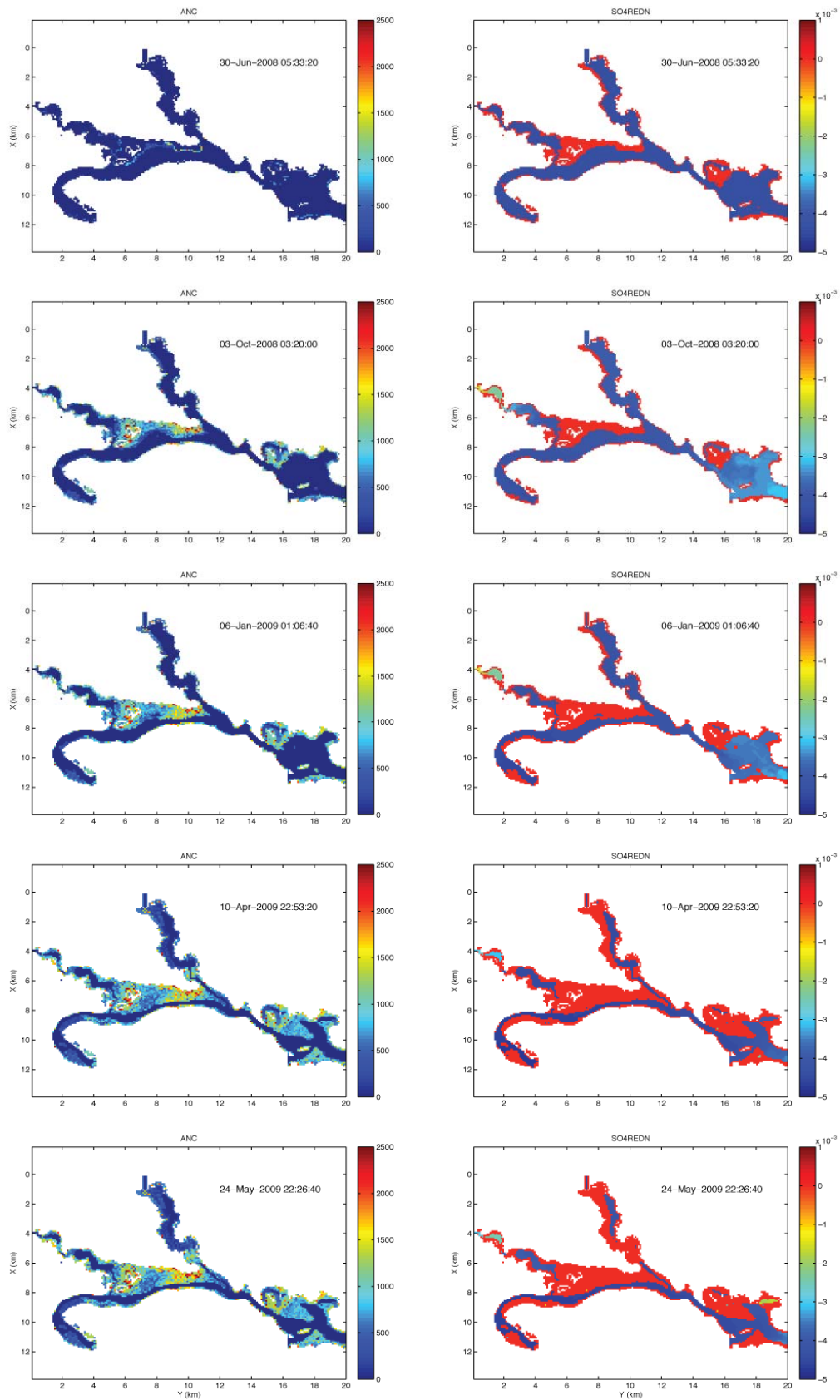


Figure 6.62: Plots of ANC ( $\text{mol H}^+ [10000\text{m}^2]^{-1}$ ) and  $\text{SO}_4$  reduction rate ( $\text{SO}_4\text{REDN}$ ,  $\times 10^{-3} \text{mol H}^+ \text{m}^{-2} \text{day}^{-1}$ ) at intervals through 2008-2009.

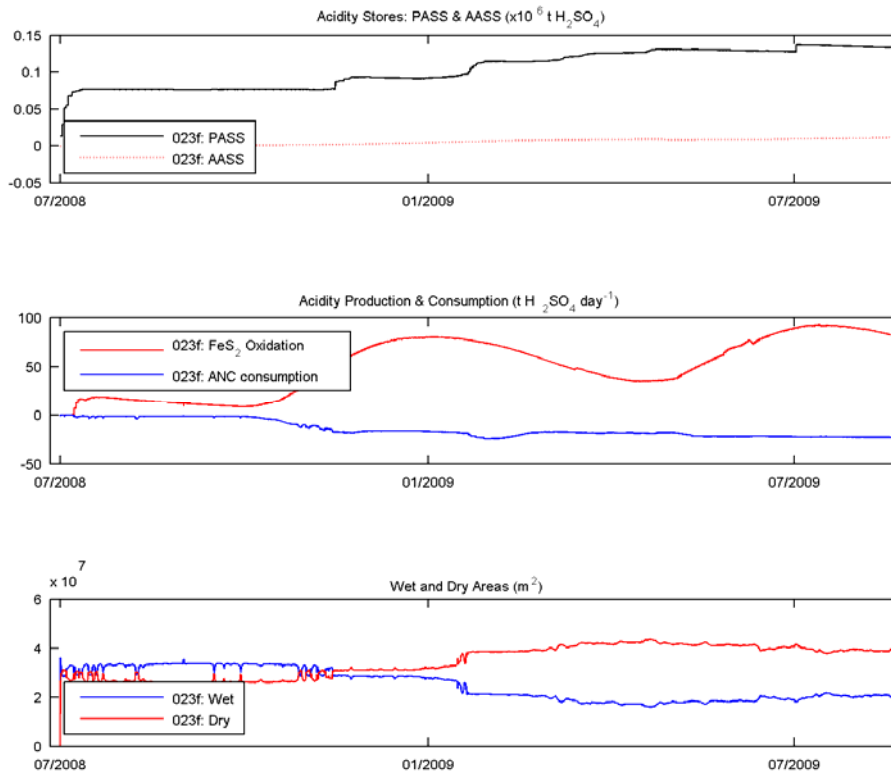


Figure 6.63a: Integrated output from the Currency/Finniss validation simulation showing accumulation of exposed PASS and subsequent AASS production and consumption.

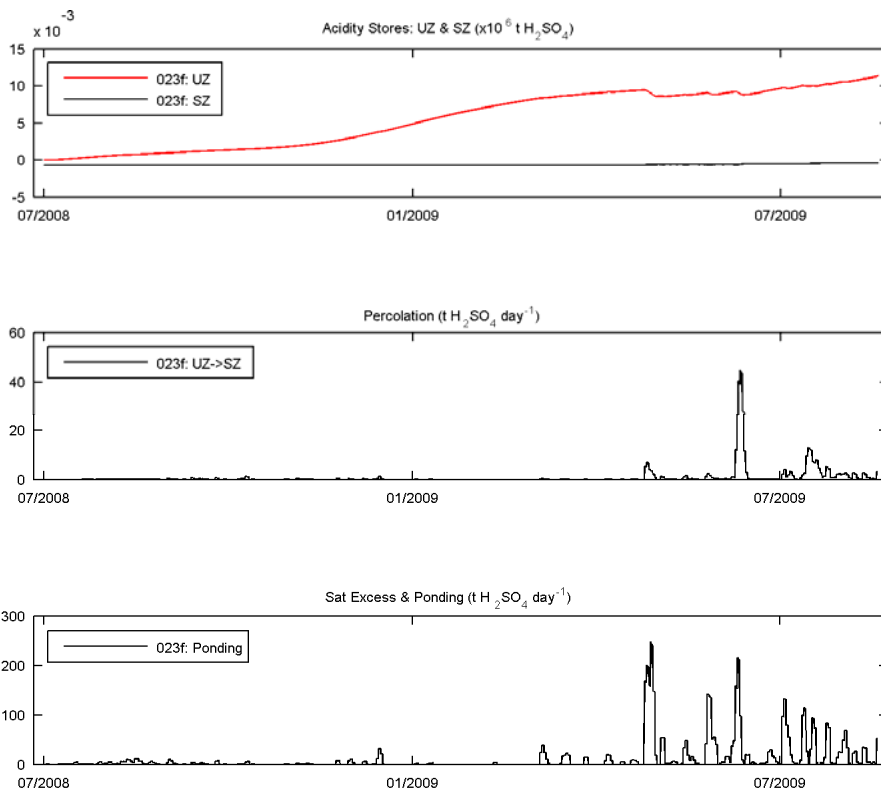


Figure 6.63b: Integrated output from the Currency/Finniss validation simulation showing the accumulation of acidity in the unsaturated and saturated zone, and process controlling mobilisation.

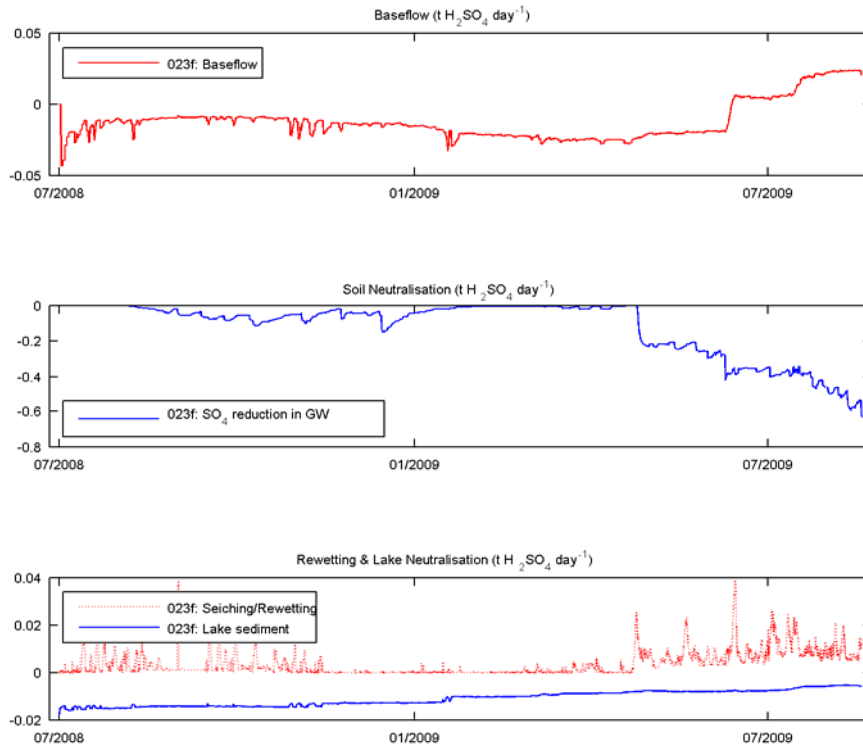


Figure 6.63c: Integrated output from the Currency/Finniss validation simulation showing the baseflow acidity flux rate, the in-soil neutralisation of acidity by sulfate reduction in the groundwater, and the rewetting flux and in-lake alkalinity flux.

An annual average budget of the key acidity fluxes and stores of acidity was compiled for the Sep 2008-Sep 2009 period to gain insights in to the dominant drivers of the acidification dynamics (Figure 6.64). These sums indicate that the amount of available acidity in the unsaturated zone is around 60,000 tonnes of  $H_2SO_4$  of which approximately 12 tonnes per day (averaged over the year) is transported to the water. The key flux process is via shallow groundwater seepage through the unsaturated zone following rainfall events, with only minor fluxes arising from the lateral movement of water within the saturated zone (-0.01 tonnes per day). This is approximately 22% of the acidity that was oxidised during the same period. A further 30% of the oxidised material was neutralised by ANC. Diffusive fluxes from rewetting and seiching are small (0.003 tonnes per day).

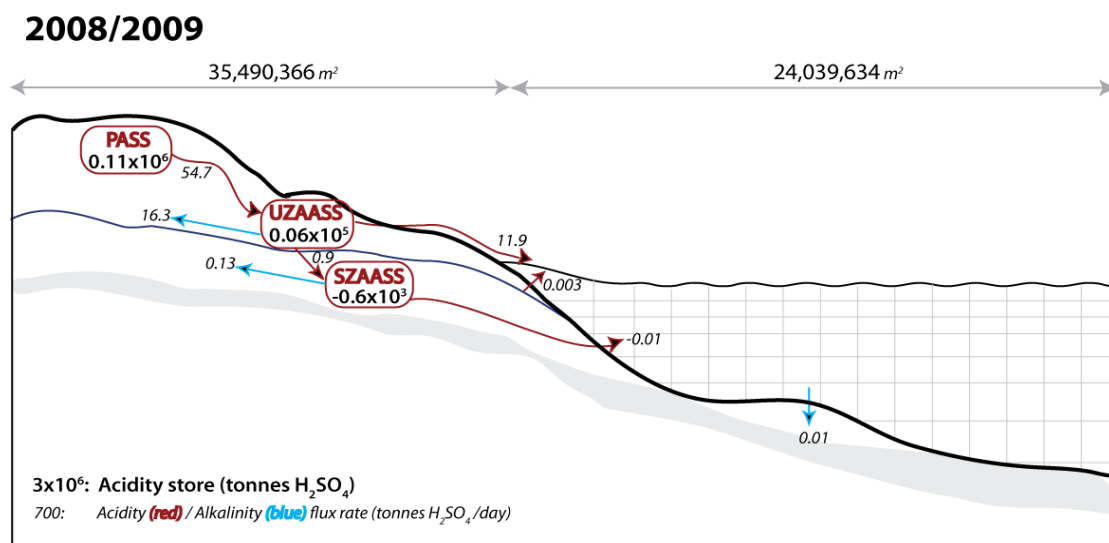


Figure 6.64: Annual average budgets of acidity stores and fluxes for Currency Creek acidification event in 2009. Data averaged over Sep 2008-Sep 2009.

